ISSN1346-7832

独立行政法人港湾空港技術研究所

港湾空港技術研究所報告

REPORT OF THE PORT AND AIRPORT RESEARCH INSTITUTE

VOL.46 NO.4 December 2007

NAGASE,YOKOSUKA,JAPAN

INDEPENDENT ADMINISTRATIVE INSTITUTION,
PORT AND AIRPORT RESEARCH INSTITUTE

REPORT OF THE PORT AND
AIRPORT RESEARCH INSTITUTE
Vol. 46 , No. 4 (12. 2007)

Behavior of Sheet Pile Quay Wall Stabilized with Sea-side Ground Improvement

M. Ruhul Amin KHAN *
Kimitoshi HAYANO **
Masaki KITAZUME ***

Synopsis

The stability of sheet pile quay walls on a thick clay deposit against *pseudo-static* and dynamic loading was studied through two series of centrifuge model tests. In the tests, a layer of over consolidated kaolin clay was prepared over a layer of dense Toyoura sand in a rectangular container. The model quay wall was set to the bottom of the sand layer. An area in the sea-side adjacent to the quay wall was improved with normal Portland cement-treated Kawasaki clay. At 50 *g* centrifugal acceleration, the clay deposit was consolidated and a cyclic horizontal line load of about 0 to 70 kN/m was applied to the quay wall in the case of *pseudo-static* loading series and four to five stages of shaking were applied to the quay wall in dynamic loading series. The width of the improved area was varied and its performance was compared with that of a quay wall embedded in unimproved ground. Results of the study indicated that the improved area provided significant resistance against static and dynamic loading. The ground improvement can reduce 30% to 60% bending moment during the dynamic loading. The horizontal deflection of the quay wall decreases rapidly with the increase in area of the CDM until it reaches a certain limit. In addition, a numerical model to estimate the mechanical behavior of the sheet pile quay wall is presented. The numerical model show good agreement with the centrifuge test results of both series.

Key Words: Sheet pile quay wall, soil stabilization, cement deep mixing, centrifuge model, numerical model, seismic load; pseudo-static load

* Dams and Geotechnical Engineer, GHD Pty Ltd., Australia (formerly, Geotechnical Engineer, Soil Stabilization Division, Geotechnical and Structural Engineering Division)

** Associate Professor, Civil Eng. Department, Yokohama National University (formerly, Senior Researcher, Geotechnical and Structural Engineering Division)

*** Director of Special Research (formerly, Head, Soil Stabilization Division, Geotechnical and Structural Engineering Division) 3-1-1 Nagase, Yokosuka, 239-0826 Japan

Phone：+81-46-844-5055 Fax：+81-46-841-8307 e-mail:kitazume@pari.go.jp

港湾空港技術研究所報告
第 46 巻第 4 号(2007. 12)

岸壁前面をセメント固化した改良地盤中の矢板の挙動

M. Ruhul Amin Khan*・早野　公敏**・北詰　昌樹***

要　旨

大型船舶への対応として既存岸壁を増深することや，大きな地震への対応として既存岸壁を耐震強化することなどが工事として行われている．その際，これまでの設計以上の外力が作用するために，なんらかの形で補強することが必要になる．既存岸壁の場合には，可能な限り機能を停止することなく補強することが必要であり，そのような場合の補強方法として，岸壁前面部を深層混合固化処理により地盤改良することが有効な方策の一つとして考えられる．しかしながら，現行の基準が対応していないために，このような地盤改良工事の設計を行う際には各現場で手探りの状態にならざるをえない．そこで本研究では，岸壁前面部を深層混合固化処理工法により地盤改良した場合の既存岸壁の補強効果について，模型実験および数値解析を実施して検討を行った．具体的には，矢板岸壁の前面を深層混合固化処理工法で改良した地盤の常時および地震時の挙動について，遠心模型実験および数値解析でモデル化を行い，改良地盤の補強効果を明らかにした．

研究の結果，改良範囲を変化させた多くの遠心模型実験の結果、矢板前面を改良することによって、岸壁の変形や矢板に発生する曲げモーメントをかなり抑制することができることが分かった。特に、粘土層厚の 1/2 程度の改良でも、全層改良に匹敵する改良効果が得られる事が分かった。また、実験結果から得られた改良範囲と岸壁天端変位、矢板に発生する曲げモーメント分布、地盤反力係数との関係を示した。地盤反力係数を用いた数値解析によって、矢板挙動に及ぼす改良効果をある程度評価出来ることを示した。

キーワード：矢板式岸壁，深層混合処理工法，遠心模型実験，数値解析，静的荷重，動的荷重

*　Dams and Geotechnical Engineer, GHD Pty Ltd., Australia（前：地盤・構造部　地盤改良研究室　特別研究員）
**　横浜国立大学大学院工学研究院　システムの創生部門　（土木工学）准教授（前：地盤・構造部　主任研究官）
*** 特別研究官（前：地盤・構造部地盤改良研究室長）
〒239-0826　横須賀市長瀬3-1-1　独立行政法人港湾空港技術研究所
電話：046-844-5055　Fax：046-841-8098　　e-mail:kitazume@pari.go.jp

Contents

1. Introduction

Steel sheet pile quay walls are designed and constructed as flexible type retaining walls to let ships berth as well as resist earth pressure of the backfill. A sheet pile quay wall is usually composed of interlocking sheet piles, tie-rods, and anchors. The wall is supported at the upper part by anchors and at the lower part by embedment in a competent soil. Typical failure modes during earthquakes depend on structural and geotechnical conditions. In the field, the structure should be designed in such a way that the induced stress and the displacement should not exceed the allowable values. But the induced stress sometimes may exceed the allowable limit rather than the displacement. Different degrees of rotation, horizontal displacement and structural failure during earthquakes are the major causes of damage to sheet pile quay walls. Sheet pile quay walls at Ohama Wharf and Shimohama Wharf of Akita Port, Japan, failed by excessive bending moment, horizontal displacement, and different degrees of rotation during the 1983 Nihonkai-Chubu earthquake (PIANC, 2001).

The seismic stability of a sheet pile quay wall can generally be improved by: (i) increasing the internal friction angle or cohesion of the backfill soil, (ii) driving the sheet pile into a dense layer of sand, (iii) replacing sheet piles, (iv) supporting the wall by additional ties or anchorages. Ohmaki et al. (2002) showed that horizontal displacement of the sheet pile top decreases as the horizontal distance between the sheet pile and anchor piles increases. Watabe et al. (2006, 2002) showed the effective seismic performance of an anchored sheet pile quay wall and a caisson quay wall backfilled with light weight materials. They performed a series of centrifuge shaking table tests for each type of quay wall. Lightweight material was composed of dredged clay, cement and very fine air foam (Watabe et al., 2004). Lightweight backfill was found effective in earthquake loading for short embedment depth sheet pile quay walls. Kitazume et al. (2002) performed a series of centrifuge model test on failure pattern and earth pressure of cement treated ground behind a caisson-type quay wall under seismic loading. The improved backfill ground reduced the earth pressure on the quay wall and the horizontal deflection of the quay wall as well. There is ample evidence from devastating 1995 Nanbu (Kobe), Hyogo ken, Japan, 1999 Kocaeli, Turkey and 1999 Chi-Chi, Taiwan earthquakes that improved sites suffer less ground deformation and subsidence than adjacent unimproved areas. The studies of the events clearly indicate that ground improvement reduces large ground displacements during seismic motion. Recently in Japan, cement treated soil has been used as a backfill material behind a sea revetment or a quay wall in which soft dredged soil is mixed with relatively small amount of cement without any compaction. Though the interaction between the improved ground and the quay wall is complicated and not yet thoroughly clarified, Tsuchida et al. (1996, 2001) investigated the dynamic earth pressure of cement treated ground and proposed a simple calculation method for practical design. Kitazume et al. (1998, 2002, and 2003) investigated the failure pattern and static and dynamic active earth pressure of cement treated soil ground by centrifuge model tests. Combination of vertical tension crack and shear failure plane was observed in the investigations.

Most of the mentioned techniques require large efforts and time, especially in the case of an existing quay wall. A sheet pile quay wall in the Chiba Port, Japan is one of the examples which requires improving its seismic stability. For an existing quay wall, it would be preferable not to close the port for a long period. The sea-side ground improvement is one of the proposed techniques which will not hamper the port-side activities during its execution, so that the service of the port is uninterrupted so long. Almost all researches on stability of quay walls are involved the above-mentioned techniques. It is considered necessary to conduct a comprehensive experimental study on the effects of sea-side ground improvement on the stability of existing sheet pile quay walls.

The sea-side ground improved with the method of cement deep mixing (CDM) (CDIT, 2002) is studied through the two series of centrifuge model tests. The stability of the improved sheet pile quay wall subjected to a number of cycles of horizontal load is investigated in the *pseudo-static* test series. The conventional practice for evaluating seismic stability of retaining walls, including gravity, sheet pile and cellular walls, is based

on p*seudo-static* approaches (PIANC, 2001). In this procedure, a seismic coefficient, expressed in terms of the acceleration of gravity, is used to compute an equivalent p*seudo-static* inertial force for use in analysis and design. The actual dynamic behavior of retaining walls is much more complex than treated in the *pseudo-static* approach. However this approach has been the basis for the design of many retaining structures in North America, Japan and other seismically active regions around the world (Whitman and Christian, 1990; Tsuchida, 1990). Stability of the improved quay wall is described in terms of structural and foundation ground behavior. A numerical method for estimating the mechanical behavior of the improved sheet pile quay wall subjected to horizontal loading is introduced. Comparison between the results of numerical calculations and centrifuge model tests is presented to validate the numerical method. Basic equation of deflection of the sheet pile is introduced and solved for boundary conditions. The numerical method can be effectively used in predicting the deflection, bending moment and shear force acting on the sheet pile quay wall. These are the important elements of structural design.

It is also considered necessary to conduct a comprehensive experimental study on the effects of sea-side ground improvement on the seismic stability of existing sheet pile quay wall. The second series of centrifuge model shaking table test is different from the *pseudo-static* test series in loading point of view. The sheet pile quay wall studied in the both series is without anchorage and tie and embedded in a thick clay deposit. An area at the sea-side adjacent to the quay wall was improved with cement-treated Kawasaki clay. At 50 *g* centrifugal acceleration, the clay ground was consolidated and four to five stages of shaking were applied to the quay wall. Sinusoidal input accelerations were ranged from 28 Gal to 343 Gal and applied at frequency of 2 Hz (100 Hz in model scale) and in 50 sinusoidal cycles. The aim of the centrifuge shaking table test is to explore the dynamic behavior of sheet pile quay wall improved with sea-side cement deep mixing (CDM).

The use of geotechnical centrifuge testing has been established as a powerful technique in the understanding of soil-structure interaction problems subjected to earthquake loading. The VELACS (VErification of Liquefaction Analysis by Centrifuge Studies) project (Arulanandan and Scott, 1993, 1994) offered a good opportunity to verify the accuracy of various analytical procedures used to predict the dynamic behavior of several bench mark problems. These problems were simulated by centrifuge tests in more than one geotechnical centrifuge. The results of the centrifuge tests conducted at different centrifuge centers were reasonable and provided a large data base against which numerical predictions may be compared. Since 1 *g* modeling of quay walls faces limitations like hydraulic condition and effective stresses in the foundation ground and requires lot of resources, centrifuge modeling is chosen to conduct the study. Centrifuge model can simulate the hydraulic condition and effective stresses in prototype.

2. Centrifuge Model Tests

Geotechnical centrifuge, Mark-II in the Port and Airport Research Institute (PARI) was used to perform the model tests. The centrifuge has an effective radius of 3.8 m, maximum acceleration of 113 *g* and maximum payload of 27.6 kN. Specifications of the Mark-II centrifuge are listed in **Table 1**. The detail of the centrifuge and surrounding equipment have been presented (Kitazume and Miyajima, 1995).

Table 1. Specifications of PARI Mark-II geotechnical centrifuge.

Specification	value
Diameter of rotating arm	9.65 m
Maximum effective radius	3.8 m
Maximum acceleration	113 *g*
Maximum payload	2760 kg
Maximum capacity	312,000 *g*.kg
Maximum rate of rotation	163 rpm
Main motor capacity	DC 450 kW

3. Pseudo-static Loaded Sheet Pile Quay Wall

3.1 Model set-up

(1) Basic concept

The relationship between the seismic active earth pressure (P_a) and horizontal seismic coefficient (k_h) obtained by Okabe's method (Okabe, 1924) is shown in schematic diagram of **Fig. 1-(i)** and **(ii)**. In the centrifuge model shown in **Fig. 1-(iii)**, similar seismic active earth pressure can be produced by applying an incremental horizontal load, F_h, on the port-side, so that the load-deflection and other characteristics in the field (**Fig. 1-(i)**) and in the experiments (**Fig. 1-(iii)**) become similar. The F_h will act as an equivalent resultant thrust from the backfill ground. The condition of level ground on both sides (**Fig. 1-(iii)**) is simulated in this study.

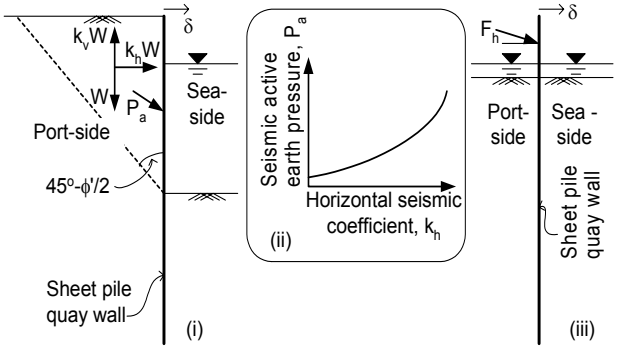

Fig. 1. Conditions of field and model quay walls.

(2) Model ground preparation

Figure 2 shows the schematic view of the model set-up. A strong box of 600 mm length, 410 mm depth and 200 mm width with a transparent front window was used for the tests. Photo of model set-up of Case 3 is shown in **Fig. 3**. The model sheet pile quay wall is a 2 mm thick steel plate instrumented with 13 pairs of strain gauges, S1 to S13, on both sides. The flexural rigidity, *EI*, of the model sheet pile wall is 1.72×10^4 kN.m. Prototype section of this plate becomes the Japanese standard sheet pile of type *SP-II* (Nippon Steel Corp., 1998). At the bottom of the strong box, the sheet pile wall was set on a 10 mm thick rough surfaced acrylic plate. At the top it was clamped with guide plates, so that it is firmly fixed and remains vertical during the model preparation.

The model sand ground of 60 mm thick was prepared by pouring dry Toyoura sand using a sand hopper. Falling height of the sand was adjusted in such a way that the relative density of the sand layer is about 90%. To saturate the sand layer, water was fed from the bottom through water supply line carefully so as not to disturb the sand layer. It took about 1.5~2 hours to saturate up to the surface of sand layer.

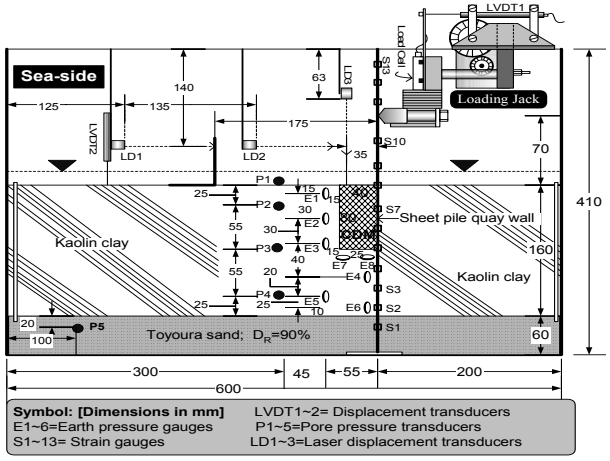

Fig. 2. Model set-up of Case 4 (in model scale).

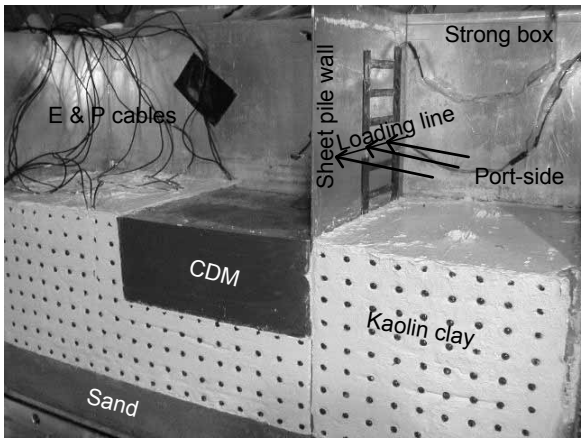

Fig. 3. Photograph of model ground (Case 3).

Table 2. Properties of kaolin clay.

Property	value
Liquid limit, W_L (%)	59.3
Plastic limit, W_P (%)	26.3
Plastic index, I_P (%)	33.0
Specific gravity, G_s	2.72
Compression index, C_c	0.49
Swelling index, C_s	0.12
Coefficient of consolidation, C_v (m^2/s)	2.5×10^{-7}
$(c_u/\sigma'_v)_{NC}$	0.314
Critical state friction angle, ϕ'_{crit}	28.61°

Table 3. Properties of Toyoura sand.

Property	value
Specific gravity, G_s	2.65
D_{10} (mm)	0.15
D_{50} (mm)	0.19
Coefficient of uniformity	1.56
Coefficient of curvature	0.96
Maximum void ratio, e_{max}	0.992
Minimum void ratio, e_{min}	0.624
Friction angle, ϕ'	42°

The kaolin clay was remolded at a water content of about 120%, approximately equal to 2 times the liquid limit and was de-aired under the negative pressure of about –90 kPa for 3 hours. A mixer incorporated with a vacuum pump was used to prepare the de-aired clay slurry. Properties of the kaolin clay and Toyoura sand are shown in **Tables 2** and **3**. On top of the saturated sand layer a filter paper of same size was placed to facilitate holding the layer of clay slurry and intactness of sand. Silicone grease was smeared on the inside walls of the strong box. The clay slurry was then poured over the saturated sand layer in the strong box with the help of a scoop. After every 30 mm slurry depth, a flat spatula was used to stir the slurry so that entrapped air bubbles dissipated and slurry became uniform.

In both the sea-side and port-side, filter paper and perforated loading plates were placed over the clay slurry. Pre-consolidation was carried out by compressing the clay with two bello-fram cylinders. The size of the perforated loading plate and filter paper in the sea-side was 398 mm × 200 mm and in the port-side 198 mm × 200 mm (**Fig. 2**). Piston of the bello-fram cylinders that incorporated a load cell (20 kN capacity) was set at the center of the loading plates and bello-fram cylinders were clamped with the strong box. A calibration chart was made beforehand which correlated the supplied air pressure to the cylinders and corresponding pressure on the surfaces of the sea-side and port-side clay. Since the loading plate covered almost all the surface of the clay and the walls of the strong box were smeared with grease, load from the pistons compressed the clay one dimensionally. The successive consolidation pressures applied were 1 kPa, 10 kPa, 30 kPa, 50 kPa, 100 kPa and 150 kPa. Primary consolidation was achieved in each stage.

After having completed the consolidation on the laboratory floor, the clay surface was skimmed off to a thickness of 160 mm. The strong box was then tilted against a wall and opened the front transparent window. Horizontal holes were drilled in specified location for inserting pore pressure transducers, P, and earth pressure gauges, E, through the clay by a small hand auger. By using guide tools, pressure transducers P and E were inserted horizontally to a depth of 10 mm. Each hole was filled with de-aired kaolin slurry. The pore pressure transducer in the sand layer was inserted near the surface carefully. Reflective blue colored beads of 6 mm diameter as optical targets were inserted through a template of 20 mm square openings (see **Fig. 3**). Before fixing the transparent window to the strong box, silicone oil was smeared on it to reduce the friction between the window plate and the front surface of the ground. The window was replaced and the strong box was set upright. The bello-fram cylinders were set again with 150 kPa consolidation pressure to recover the swelling and sensors holes.

After releasing the pressure a specified area in sea-side adjacent to the sheet pile was excavated. For example, in Case 3 the excavated area for CDM was 200 mm × 80 mm (**Fig. 3**). Cement treated Kawasaki clay which is called in this paper as CDM was poured into the excavation with the help of a spoon. Kawasaki clay slurry with 130% water content was thoroughly mixed with Portland cement. Amount of Portland cement added was 40% of dry weight of Kawasaki clay. After filling the excavation, sufficient water was added on top of the clay and CDM for curing. At least seven days curing was allowed to gain sufficient strength (unconfined compression strength, q_u, T**able 4**) by the CDM. The unconfined compression tests on CDM samples (height = 100 mm and diameter = 50 mm) were carried out according to the standards of Japan Geotechnical Society (JGS, 2000) laboratory shear test. The strain controlled compression apparatus sheared the sample at strain rate of 1% per minute. Variation of curing period which ranged from 7 to 12 days and error in exact proportioning of Portland cement and Kawasaki clay in preparing the CDM affected the q_u values that reported in **Table 4**.

Table 4. *Pseudo-static* test conditions in prototype scale.

Test cases	Case1	Case 2	Case 3	Case 4	Case 5	Case 6	Case 7
Clay depth (m)	8	8	8	8	8	8	8
CDM zone (m^2)	0×0	10×8	10×4	2×4	4×4	8×2	4×2
No. of load cycle	4	4	5	5	5	5	5
Max. load kN/m)	47	62	65	70	68	64	66
q_u of CDM (kPa)	-	920	617	1173	1536	1333	1020

Four holes were drilled with a 10 mm diameter steel pipe (a kind of sampler) in the clay at four corners of the strong box. Clay samples of every 20 mm depth from top to bottom of the clay layer were taken from each corner hole. Consistent water content and undrained shear strength profiles were determined from the clay samples along the clay depth. Acrylic pipes of 10 mm inside diameter were inserted in each of the corner hole up to the bottom sand layer. These pipes connect the top water layer and the bottom sand layer.

Laser displacement transducers, LDs, and linear Variable Displacement Transducers, LVDTs, were firmly set on top of the strong box as shown in **Fig. 2**, for monitoring the displacement of the CDM and clay, and the vertical movement of the ground surface and deflection of the sheet pile wall at loading point.

3.2 Test procedures and conditions

(1) Test procedures

The strong box with the model was mounted on the swinging platform of the centrifuge. Centrifugal acceleration was increased up to 50 *g*. The consolidation in the centrifuge at 50 *g* was conducted until the degree of consolidation was estimated to have achieved 90%. At 50 *g*, a horizontal line load was applied gradually by the loading jack to the sheet pile quay wall in the seaward direction (**Fig. 3**). As shown in **Fig. 4** loading cycles were increased from 16 kN/m to 70 kN/m. Each cycle comprised 6 turns of loading and unloading with the jack speed of 3 mm/min.

Deflection of sheet pile quay wall, vertical movements of the ground surface at the sea-side, earth pressures at various elevations and strains on the surface of the sheet pile wall were monitored. The positions of the sensors are shown in **Fig. 2**. Still pictures of the model were taken in every turn of a loading cycle for observing the deflection of the wall and displacement of ground with respect to the targets' movement.

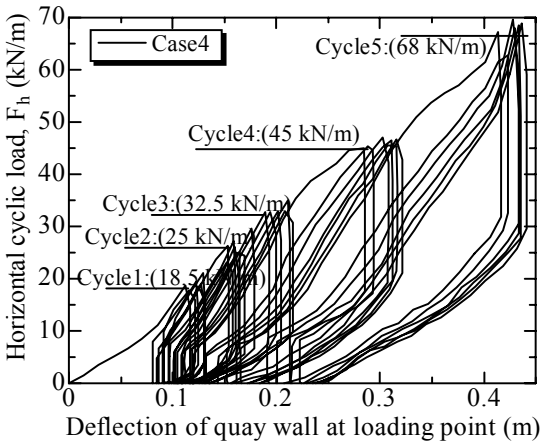

Fig. 4. Cyclic load applied to the quay wall in Case4.

(2) Test conditions

In this paper, the results of seven centrifuge tests are presented to discuss the effects of the sea-side ground improvement on the stability of the quay wall in *pseudo-static* condition. The test conditions in the prototype scale are shown in **Table 4**. All of the test cases are identical except for the size of the CDM block and the position and number of sensors. Stability of unimproved and improved sea-side ground has been examined from the unimproved case (Case 1) and the improved cases. The effect of width of the CDM block is investigated from Cases 3, 4 and 5, which have the depth of CDM equal to 4 m, and Cases 6 and 7, which have the depth of CDM equal to 2 m. Having the same width of CDM, the influence of the 'floating type' and full-depth CDM block is likewise examined from Cases 2 and 3. CDM blocks in Cases 5 and 7 also have the same width but different depth. Cross-sectional area of CDM block in Cases 4, 7 and in Cases 5, 6 is same. All the test results in the following sections are presented in the prototype scale.

3.3 Stress-strength profile of clay stratum

The seashore consists of a thick clay layer underlain by a sand layer. Highly overconsolidated clay was chosen to facilitate the model preparation and to model the quay wall numerically. The maximum effective past pressure experienced by the clay can be assumed to be the same as that applied to consolidate the clay, i.e. 150 kPa. Two saturated specimens of Toyoura sand were tested in drained triaxial compression test (JGS, 2000, relative density: 80%; σ_3': 100- 200 kPa; σ_1': 500- 760 kPa) and three kaolin clay specimens were tested in undrained triaxial compression tests (JGS, 2000, σ_3': 20- 72 kPa; σ_1': 80- 235 kPa) to obtain the critical state parameters of sand and clay. Here σ_3' and σ_1' are effective lateral and vertical stress respectively. The sheet pile was set-up to a certain depth into the strata of sand underlying the clay to ensure firm fixity of the quay wall. Stress history of the clay layer is shown in **Fig. 5**. In the figure, σ_v' and σ_p' are the current effective vertical stress and the past maximum vertical consolidation pressure respectively; *OCR* is the overconsolidation ratio (σ_p'/σ_v'); the coefficient of in-situ earth pressure, K_0, was derived for overconsolidated (OC) clay with a critical state friction angle ϕ'=28.6^0, following the equation presented by Mayne and Kulhawy (1982):

$$K_{0(OC)} = (1-\sin\phi')OCR^{\sin\phi'} \tag{1}$$

The undrained shear strength, c_u, of the clay was derived from the formula of Wroth (1984):

$$\frac{c_u}{\sigma_v'} = \left(\frac{c_u}{\sigma_v'}\right)_{NC} OCR^{\,m} \tag{2}$$

where *NC* = normally consolidated clay, with an experimental value of $(c_u/\sigma_v')_{NC}$ = 0.314 and m = 0.75(=(C_c-C_s)/C_c; see **Table 2**). Theoretical c_u values have been compared with the test results. The c_u values were computed from the water content profile along the depth both in the sea-side and port-side. After stopping the centrifuge, a few hours have passed before sampling for water content. Some swelling may have taken place in this period, which may result in a smaller c_u values than those predicted by theory. The c_u trend of Case 7 shows little larger than that of theory and other test cases. Sampling of water content in this case was done within half an hour period after stopping the centrifuge. Although the clay samples were excavated after the test, the values derived from the test results compared fairly well with the theoretical c_u values (**Fig. 5**), which were predicted before the loading stage.

3.4 Force equilibrium analysis

Forces applied to the sheet pile quay walls due to seismic motion are shown in **Fig. 6**. Unimproved case is considered with the same backfill sand as used in the bottom sand layer. Horizontal load, F_h of 70 kN/m is equivalent to a dynamic active earth pressure derived from a 7 m depth backfill which is experiencing a seismic motion with horizontal seismic coefficient, k_h equal to 0.2. Various parameters of the backfill, sand layer, clay, sheet pile wall and CDM are listed in **Table 5**. The *pseudo-static* numerical analysis presented here is

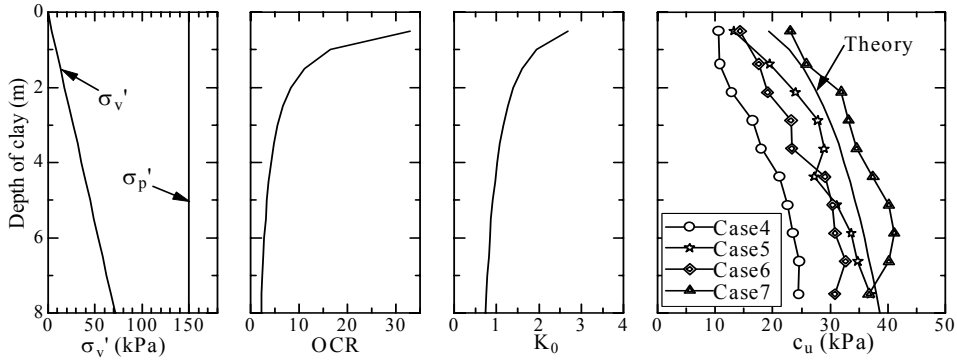

Fig. 5. Stress history of the clay stratum.

based on the Okabe's method (Okabe, 1924). The value of k_h is assumed as 0.25. Dynamic active earth pressure (summation of static and incremental active earth pressure), dynamic passive earth pressure, and hydrodynamic pressure are shown in the figure. Larger passive force is developed due to long embedment depth of the quay wall. Although in force equilibrium point of view the quay wall is safe, i.e. resisting force, 1,643 kN is greater than driving force, 908 kN, it is unsafe in overturning about its toe. Resisting moment (M_r) obtained about toe is 5218 kN.m and driving moment (M_d) is 7540 kN.m. These values give a rotational factor of safety, *Fs* (=M_r/M_d) equal to 0.69.

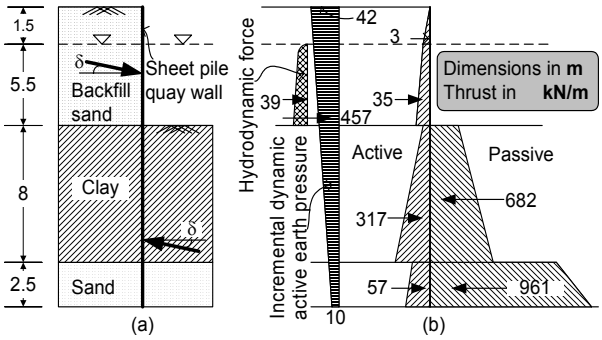

Fig. 6. *Pseudo-static* force equilibrium in unimproved case (Case 1) at k_h=0.25.

Table 5. Parameters used in pseudo-static numerical analysis.

(a) Backfill and Bottom sand

γ_{sat} (kN/m^3)	19.6
γ_{wet} (kN/m^3)	15.9
γ' (kN/m^3)	9.8

(b) Clay Stratum

γ_{sat} (kN/m^3)	18.8
γ' (kN/m^3)	8.9
c_u (kN/m^2)	25

(c) Steel Sheet Pile Wall

I (m^4/m)	8333×10^{-8}
E (kN/m^2)	2.1×10^{8}
EI (kN.m)	17170

(d) CDM Zone

γ_{sat} (kN/m^3)	15
γ'(kN/m^3)	5.2
c_u (kN/m^2)	460

Figure 7(a) shows the variation of active earth thrust with the k_h and **Fig. 7(b)** shows the variation of *Fs* with k_h for both unimproved and improved cases. In calculating the forces in improved case (Case 3, CDM=10×4 m^2) a CDM layer of 4 m depth is assumed in the clay layer which produced passive pressure like the clay ground. Since the CDM in Case 3 has maximum width, it shows the highest factor of safety which is roughly 6 times larger than that of unimproved case (Case 1). All other cases will fall in between these two lines. Interaction among the CDM, the clay and the sheet pile wall should be taken into account in calculating the cases with intermediate sizes CDM.

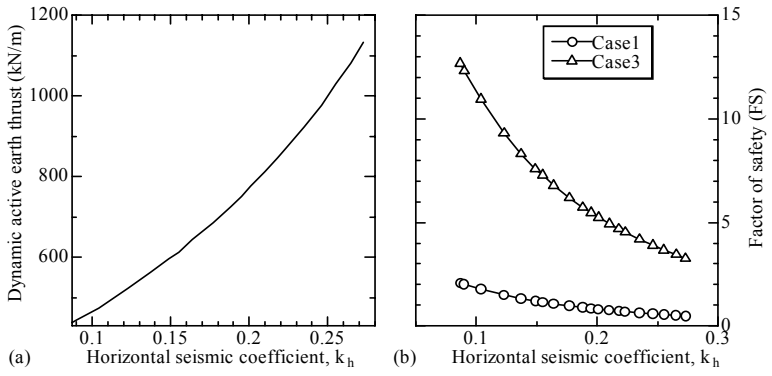

Fig. 7. Dynamic active earth thrust and factor of safety versus horizontal seismic coefficient, k_h.

3.5 Numerical method

(1) Formation of equations

Elastic equilibrium of forces acting on the horizontal slice of sub-divided layers below the ground level is considered. Portion of the sheet pile quay wall above the ground level is treated simply as a cantilever beam where lateral distributed pressure, P acting on it. In simulation of the centrifuge model condition P is assumed to be zero and a concentrated force F_h is applied at 3.5 m above the ground level. **Figure 8** schematically shows the position of F_h and sub-divided layers in the clay stratum. Since coefficient of horizontal subgrade reaction, k_s value of the bottom sand layer is much larger and not sensitive to the predicted deflection, sub-division in sand layer is not necessary. As earlier stated, the F_h is the equivalent dynamic active earth thrust. In actual field condition P can be a polygonal pressure distribution. According to the theory of elastic beam, equation of deflection, y of the sheet pile quay wall above the ground level,

$$EI\frac{d^4y}{dx^4} = P \tag{3}$$

where EI is the flexural rigidity of the sheet pile, x is the vertical coordinate of elevation as shown in **Fig. 8**. General solution of Eq. (3) is obtained as:

$$y = A_1x^3 + A_2x^2 + A_3x + A_4 + Qx^4 \tag{4}$$

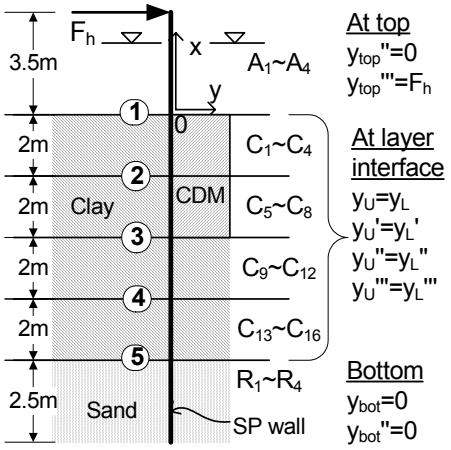

Fig. 8. Numerical model of sheet pile quay wall.

where A_1~A_4 are integral constants obtained from the boundary conditions and Q= $P/(24EI)$. Behavior of sheet pile quay wall below the ground level is modeled by the method of horizontal subgrade reaction (Chang, 1937). Underground deflection of the sheet pile quay wall can be expressed as:

$$EI\frac{d^4y}{dx^4} = -k_s y \tag{5}$$

where k_s is the coefficient of horizontal subgrade reaction on the sheet pile wall. General solution of Eq. (5) is obtained as:

$$y = C_ie^{\beta x}\cos\beta x + C_je^{\beta x}\sin\beta x + C_ke^{-\beta x}\cos\beta x + C_le^{-\beta x}\sin\beta x \tag{6}$$

where $\beta = \sqrt[4]{k_s/(4EI)}$, C_i ~ C_l are integral constants obtained from the boundary conditions in each layer of the clay ground (≈ C_1 ~ C_{16} are used in the application). Similar general solution can be written as Eq. (7) for the sand layer with the integral constants R_1 to R_4.

$$y = R_1e^{\beta x}\cos\beta x + R_2e^{\beta x}\sin\beta x + R_3e^{-\beta x}\cos\beta x + R_4e^{-\beta x}\sin\beta x \tag{7}$$

(2) Boundary conditions and solutions

To put the appropriate value of k_s to the equations, the clay ground has been divided into four layers. Number of layers can be varied according to field conditions and required degree of accuracy of the prediction. Properties of the ground, sheet pile, CDM and average k_s values for each layer are shown in **Tables 4** and **5**. As shown in **Fig. 8**, integral constants used in this model are A_1~A_4, C_1~C_{16} and R_1~R_4. In the figure, y, y', y'', y''', y'''' represent zero, 1st, 2nd, 3rd, and 4th degree of derivative whose respective physical meanings are deflection, angle of deflection, bending moment, shear force and distributed load on the sheet pile quay wall. At the top of the wall: y_{top}''= 0, y_{top}'''= F_h, P = 0 and two equations are formed with constants A_1~A_4. Left hand sides of these two equations are the 2nd and 3rd derivative of Eq. (4). At each of the five

layer-interfaces, four equations are formed with the following boundary conditions: $y_U = y_L$, $y_U' = y_L'$, $y_U'' = y_L''$, $y_U''' = y_L'''$; where '$_U$' represents upper layer and '$_L$' the lower layer of a particular layer-interface. In layer-interface 1 (ground level), different degrees of derivative of Eqs. (4) and (6) are set on both sides of the boundary equations. A_1~A_4, and C_1~C_4 appears in the interface 1. Likewise C_1~C_{16} and R_1~R_4 are appeared in the equations of the remaining interfaces. In the five layer-interfaces, twenty equations are formed. At the bottom of the wall: $y_{bot} = 0$, $y_{bot}'' = 0$ and two equations are formed with constants R_1~R_4. Left hand side of these boundary conditions is the zero and 2nd derivative of Eq. (7). Twenty four unknowns are then derived from the set of twenty four equations. Particular solutions are obtained by using these constants (unknown) to the equation of deflection in each layer. Successive differentiations of deflection equations give the corresponding bending moment, shear force and load distribution on the quay wall.

3.6 Results and discussions

(1) Centrifuge consolidation and pore pressures

Data from the pore pressure transducers, P, and LVDT2 in the clay were used to estimate the degree of consolidation at 50 *g* prior to the loading stage. Square root of time method was used to estimate the degree of consolidation. Time taken to achieve 90% consolidation in the centrifuge was about 4.5 hours. Since the depth of the clay stratum in all cases is the same (8 m), almost the same amount of consolidation settlement was observed. This highly overconsolidated clay stratum was found to settle about 0.40 m in the prototype scale. The consolidation process makes the soil a competent foundation with definite stress history.

Pore pressure responses during centrifuge consolidation in Cases 4 and 5 are shown in **Fig. 9**. As seen from the figure, the foundation ground came to the state of equilibrium by continuous dissipation of the pore pressure. Pore pressure transducer, P4, which was placed near the bottom of the clay stratum (see **Fig. 2**), dissipated larger pore pressure than that of P3 and P2. The response from P1 and P5 are almost flat which were placed at the ground surface and at the bottom sand layer respectively. This indicates that constant hydrostatic pressure is available at the boundaries of the clay stratum during the test. Theoretical hydrostatic pressures are given in brackets in the figure. At the end of consolidation, sudden rise of pore pressure of P2 in Case 5 is observed. Slightly settle down of the transducer from its original position may cause this rise. Responses from the pore pressure transducers are satisfactory.

Excess pore pressure in the ground may affect the stability of the sheet pile quay wall significantly. Almost constant equilibrium pore pressure from each of the pore pressure transducers was observed during the loading stage.

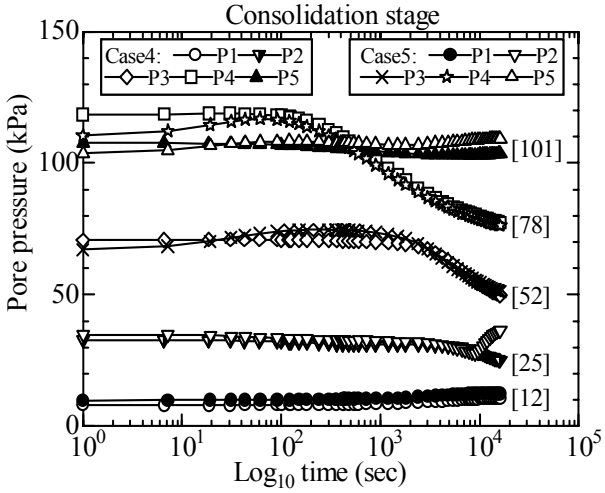

Fig. 9. Dissipation of excess pore pressure during centrifuge consolidation stage (Cases 4 and 5).

(2) Deflection of sheet pile quay wall

Deflection of the quay wall is the main index in describing stability. **Figures 10 (a)** and **10(b)** show the in-flight photo of Case 4 at the initial stage and 68 kN/m loading stage respectively. Various elements are marked in the figures. Some deflection of the sheet pile wall from vertical position can be seen in **Fig. 10(b)**.

Figure 11 shows the relationship between horizontal load, F_h, and deflection of quay wall at loading point. Deflection at F_h = 45 kN/m, δ_{45}, is chosen to compare with the data of all cases and is tabulated in the figure. Deflection δ_{45} of the unimproved ground of Case 1 is 0.47 m whereas full-depth CDM improved ground of Case 2 is 0.12 m. Improved stiffness becomes almost four times larger than that of the unimproved sea-side ground. Here stiffness is indicated as horizontal load

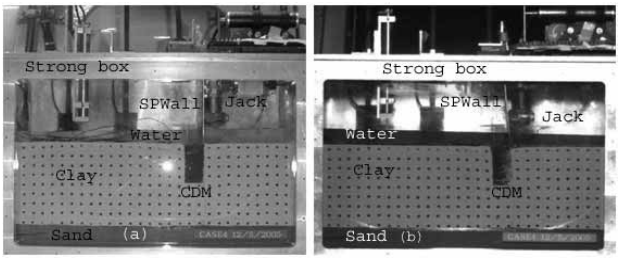

Fig. 10. In-flight photo of model sheet pile quay wall of Case 4 showing: (a) initial condition before applying the load and (b) at the 68 kN/m loading stage.

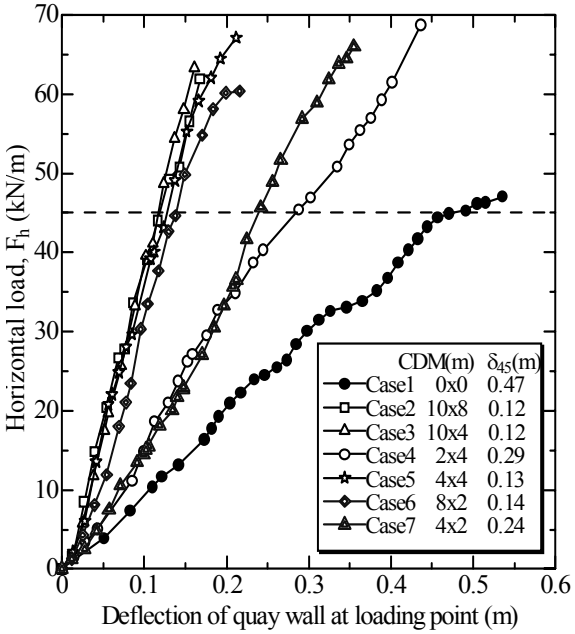

Fig. 11. Load deflection curves of the sheet pile quay wall.

per unit deflection. Cases 4, 5, and 3 with the same depth of CDM (depth: 4 m) but different width (respective widths: 2 m, 4 m and 10 m) have δ_{45} of 0.29 m, 0.13 m and 0.12 m respectively. Even though the width in Case 3 was more than double that of Case 5, the deflection was not decreased proportionally as decreased in Cases 4 and 5. The results indicate that in increasing the width or size of the CDM to the full depth of the clay, a small amount of deflection of the quay wall will take place. This is defined here as the limit of least deflection.

Cases 7 and 6 with the same depth of CDM (depth: 2 m) but different width (respective widths: 4 m and 8 m) have δ_{45} value of 0.24 m, and 0.14 m respectively. The stiffness offered by the quay wall in these cases is almost proportional with the width of CDM. However, the interaction between the quay wall and the CDM, and between the CDM and the surrounding clay are not yet thoroughly investigated. These interaction processes can affect the deflection of the quay wall significantly. Cases 2 and 3 having floating or half-depth and full-depth CDM (with the same width of treated material) have δ_{45} value of 0.12 m in each case. Increasing the depth of CDM may have stiffened the ground and reduced the wall deflection towards the limit of least deflection. The effect of the depth of CDM is also investigated from Cases 5 and 7 which have the same width but different depth show δ_{45} of 0.13 m and 0.24 m. Deflection is increased about double in the case with smaller depth CDM. Sectional-area wise performance of the CDM can also be compared from Cases 4, 7 and Cases 5, 6. Cases 4 and 7 having the same cross sectional-area (= 8 m^2) show δ_{45} values of 0.29 m and 0.24 m. And Cases 5 and 6 (area = 16 m^2) show δ_{45} values of 0.13 m and 0.14 m. Almost the same δ_{45} values are observed in each group.

(3) Earth pressures

Horizontal and vertical earth pressures around the CDM block and sheet pile quay wall indicate the mechanism of deflection of the quay wall. Due to increasing the horizontal load, F_h, shear deformation of the foundation ground starts to take place. Gradual increasing trend of total horizontal pressure, σ_h, in the sea-side was observed during the loading stage. Variation of shearing stress ratio, $(\sigma_h-\sigma_v)/2c_u$ with the applied horizontal load, F_h is shown in **Fig. 12**. Here σ_h and σ_v are the total horizontal and vertical earth pressure respectively. The values of σ_h are obtained from the earth pressure gauges, E, placed along the depth and the values of σ_v are calculated by considering the parameters shown in **Table 5**. The c_u values are determined from the water content profile of the clay as stated in **Fig. 5**. With the deflection of the quay wall, shearing among the CDM block, sheet pile wall and the surrounding clay takes place. Similar rising trends of shear stress ratio are found in the clay. This indicates a uniform shearing resistance offered by the clay against the horizontal loading. The ratio ranges from -0.3 to +0.4.

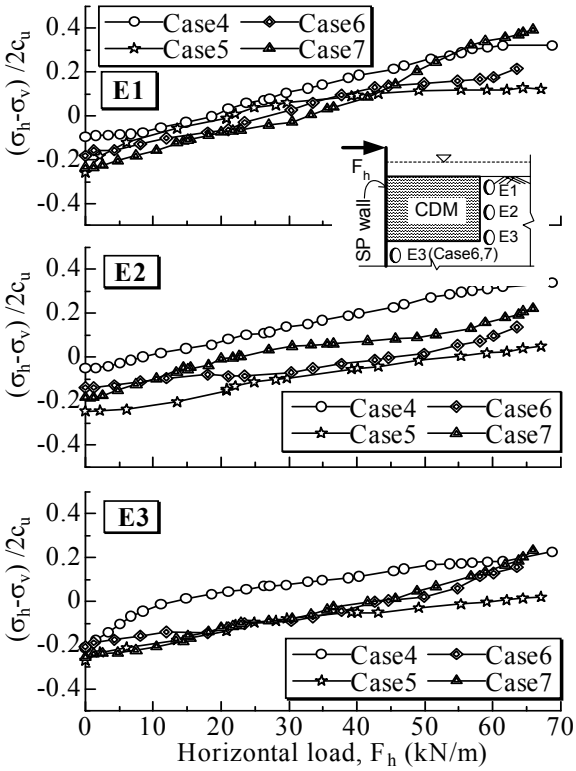

Fig. 12. Variation of shear stress ratio, $(\sigma_h-\sigma_v)/2c_u$, with the applied horizontal load, F_h.

Earth pressure gauges (E1~E6) along the CDM block and sheet pile wall measure the horizontal earth pressure. **Figures 13(a)** and **13(b)** show the distribution of horizontal earth pressure at initial condition and F_h = 45 kN/m loading condition respectively. Theoretical distributions of active, passive and K_0 earth pressures (EP) are shown in the figures. Position of earth pressure gauges is shown in the inset of the figure in model scale. Changes of earth pressure are more prominent in shallower part than in deeper part. At initial condition (**Fig. 13(a)**) earth pressure distributions in the top part of the clay are lying near the K_0 line. Due to the consolidation settlement, the bottom part is compressed more than the top part and the earth pressure condition has started to change from the K_0 to passive state. Surface roughness of the CDM block and the sheet pile wall can also affect the K_0 earth pressure. Noticeable changes in earth pressure distributions can be seen in the loading condition (**Fig. 13(b)**). Earth pressures of all cases almost lie on the line of passive pressure. With the deflection of the quay wall the earth pressures at the sea-side reach to the passive state.

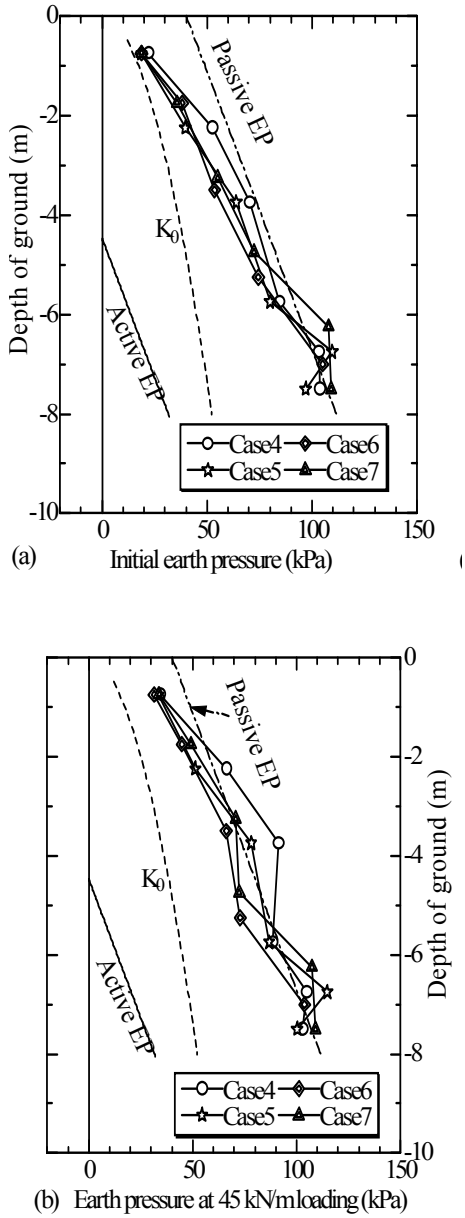

Fig. 13. Earth pressure distribution on the sheet pile quay wall: (a) initial condition and (b) during the 45 kN/m loading stage.

(4) Rotation of the CDM

Figure 14 shows the response of vertical earth pressure below the CDM block at the F_h = 45 kN/m loading stage. Earth pressure gauges (E7~E8) were set below the CDM to measure the vertical pressures. Rotation of CDM block during the loading stage can be understood by comparing the initial (ini.) and final values of vertical earth pressure. Due to the effect of friction between the improved ground and the sheet pile

wall during consolidation, the CDM block tends to rotate more when its width or size reduces. Initially the value of the outer earth pressure gauge (E7) becomes a little larger than that of the inner earth pressure gauge (E8, which closer to the sheet pile wall) due to the stated friction effect during consolidation and gradual rise of water level in the seaward direction at 50 *g* (see water level in **Fig. 10**). All of the cases show the deviation from the initial line with an indication of the seaward rotation of the CDM block.

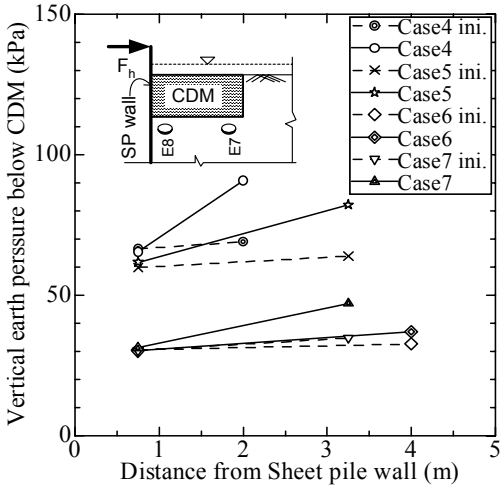

Fig. 14. Vertical earth pressure observed below the CDM block at the initial (ini.) and the 45 kN/m loading stage.

Movement of the CDM block during the loading stage was monitored by the laser displacement transducers (LD2 and LD3, **Fig. 2**). **Figures 15(a)** and **15(b)** show the horizontal and vertical displacement of a point on the CDM block with the applied load, F_h. The monitored point is *(7/8)W* away from the sheet pile wall (see the inset figure). Here *W* is the width of the CDM block. Maximum horizontal displacement, δ_h and maximum vertical displacement, δ_v of all cases are also shown in the figures. Since horizontal displacement of the CDM is directly related with the magnitude of F_h and the flexural rigidity of the sheet pile wall, relatively larger value of δ_h is observed. The maximum horizontal displacement of the CDM is about 30% of the maximum horizontal deflection of the sheet pile wall. Horizontal displacement in Cases 2 and 3 is found to negligible values. Case 4 with the smallest width CDM shows larger displacement both horizontally and vertically.

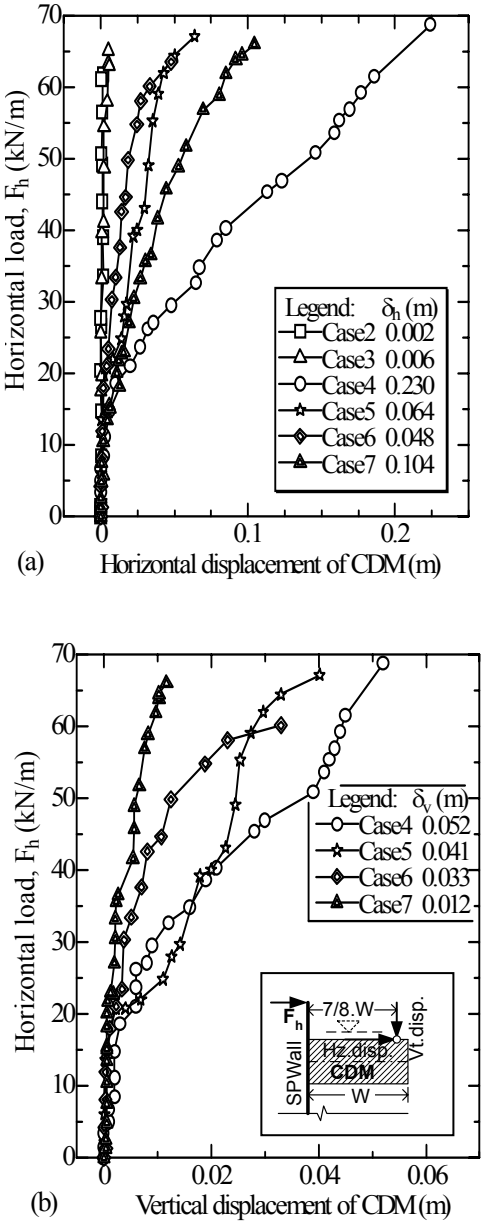

Fig. 15. Movement of the CDM block during the loading stage: (a) horizontal displacement and (b) vertical displacement of the CDM block.

Vertical displacement observed of the CDM is about 40% of its horizontal displacement. Friction between the sheet pile wall and the CDM block, interaction between the CDM and the surrounding clay and size of the CDM affect the degrees of rotation. Cases 4 and 5 with 4 m depth CDM show larger vertical displacement

than that of Cases 6 and 7. **Fig. 15(b)** indicates, cases with smaller depth CDM (Cases 6 and 7) are more efficient than those with larger depth. Resultant displacement of the CDM block can be determined from its horizontal and vertical displacement components. Resultant displacement at the outer edge of the CDM supports the rotation of the CDM block.

(5) Strength of the CDM

Unconfined compression test of the same CDM as used in each case was carried out to determine the strength, q_u. The q_u value which ranges from 610 kPa to 1,540 kPa is shown in **Table 4**. Average water content variation in the CDM is about 85% at the top and about 75% at the bottom. Needle penetration tests were carried out on both of the contact faces of the CDM block (sheet pile wall side and the clay side). Needle penetration tests were carried out at each node of a 1 cm squared mesh that was drawn in both contact faces of the CDM. Needle penetration instrument is a treated soil testing apparatus (type: *SH-70*, capacity: *100 N* Maruto Testing Machine Company Ltd., Japan) where a 1 mm diameter needle is penetrated to 10 mm into the CDM. Corresponding strength is measured from a sliding ring over a scale of N/mm. This strength is then converted into kPa ($\approx q_u$) with the help of a calibrated relationship obtained from a series of CDM samples of different clay-cement ratio. The strength contours on both faces of the CDM show that the strength in the top

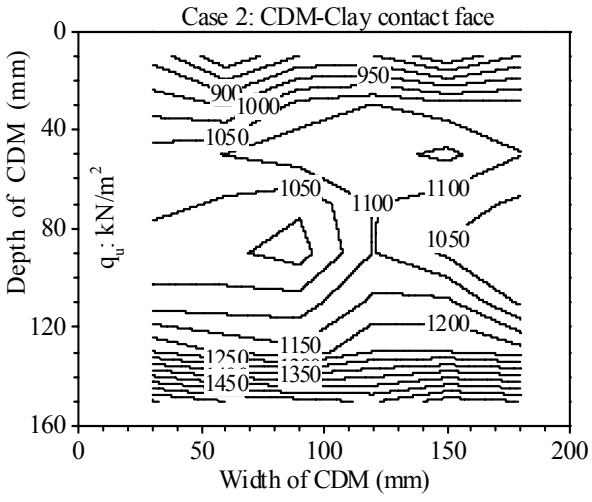

Fig. 16. Strength contours of CDM at the clay contact face obtained from needle penetration test in Case 2.

part of the CDM block is about 900 kPa and in the bottom part is about 1,550 kPa (shown in **Fig. 16**). Since the water layer was always on top of the CDM block, relative water content in the top part becomes larger and results in smaller strength than that of the bottom part. Both contact faces of the CDM show same strength variation, larger in the bottom part and relatively smaller in the top part.

(6) Bending moments and deflection

Bending moments are derived from the responses of the strain gauges (S) along the sheet pile wall (see **Fig. 2**). **Figures 17(a)** and **17(b)** show the bending moment and deflection distribution of the sheet pile quay wall at the 45 kN/m loading stage derived from centrifuge tests and numerical method. By using the particular solutions from the numerical method, bending moment, deflection distribution, shear force and distributed horizontal load to the quay wall are determined for the conditions of each centrifuge model test (**Table 4**). Test data of bending moments are shown as dashed line in **Fig. 17(a)** and the numerical predictions are shown with solid lines (**Figs. 17(a)** and **17(b)**). Almost similar pattern of bending moment is developed in all cases. Unimproved case (Case 1) shows the maximum bending moment of 215 kN-m below the ground level whereas the cases with improved sea-side ground show nearly half of this value. Maximum bending moments in the improved cases take place at the ground surface. Maximum bending moments in the cases with CDM depth equal to 4 m ranges from 120 to 130 kN-m and in the cases with CDM depth equal to 2 m ranges from 125 to 150 kN-m. The trends of Cases 4 and 7 which have the smallest size CDM show a curvature like the unimproved case. Small negative bending moments are also observed at the bottom part of the sheet pile wall. Case 3 shows the least bending moment and deflection.

The CDM is relatively much stiffer than the surrounded clay. The top part of the CDM adjacent to the sheet pile quay wall resists F_h primarily and distributes it to the surrounding clay. Due to firm fixity in the bottom dense sand, the sheet pile wall tends to bend more at the ground surface in all of the improved cases. Interaction among the CDM, the sheet pile wall and the clay reduces the bending moments according to the size

of the CDM block. Since k_s represents the reaction of ground to the wall and was considered the appropriate value in each layer of the ground, the prediction of bending moment and deflection becomes reasonable (**Figs. 17(a)** and **17(b)**). Though the magnitude of bending moment shows some differences from the numerical prediction, the shape and overall profile agree well with the numerical method.

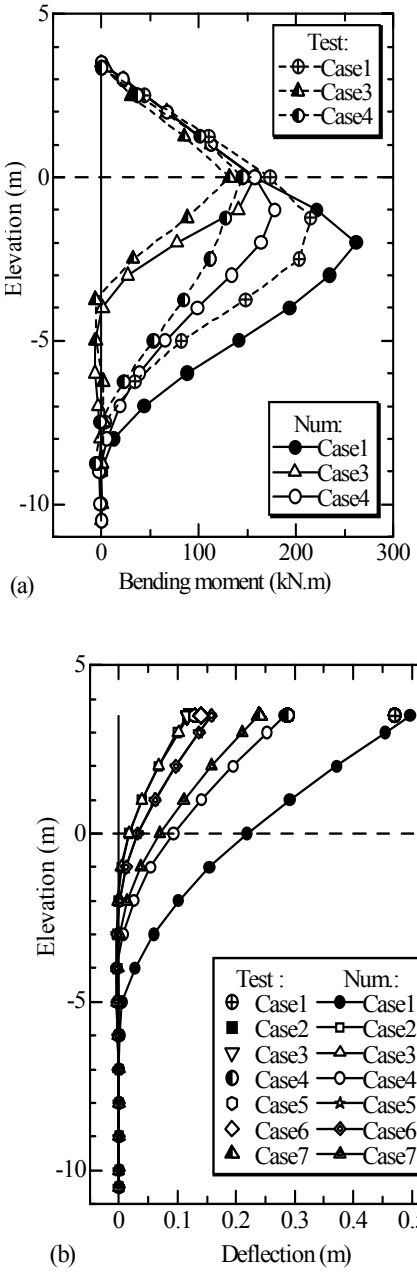

Fig. 17. Bending moments and deflection distributions of the sheet pile quay walls at the 45 kN/m loading stage.

Deflection at the loading point which is 3.5 m above the ground level was recorded at 45 kN/m loading and is shown in **Fig. 17(b)** as test data. Firm fixity at the bottom part, gradual bending near the ground surface and maximum deflection at the top can be visualized from the deflection distribution of the sheet pile quay wall. Deflection distributions of the sheet pile quay wall show good agreement with the test points.

(7) Horizontal subgrade reaction

Quantic spline functions were used to fit the bending moment test points in **Fig. 17(a)**. Two successive differentiations of spline-curve of the bending moment distributions give the horizontal subgrade reaction on the wall below the ground level which is shown in **Fig. 18(a)**. Maximum subgrade reaction is observed at the ground level and it reduces toward the bottom of the sheet pile quay wall to zero or very small value. Maximum subgrade reaction in the unimproved case (Case 1) is found as -12 kN/m^2/m whereas in the improved cases it ranges from -60 kN/m^2/m to -125 kN/m^2/m. Since the subgrade reaction geometrically represents the curvature of the bending moment distribution, it is very sensitive to any fluctuation of the bending moment at a given depth and therefore strongly depends on the choice of the fitting curve of the bending moment (King, 1994). Although the trends from spline equations are seen as zigzag, it should be smooth nonlinear curves.

Figure 18(b) shows the plot of horizontal subgrade reaction versus displacement at the ground surface. Average trend line is shown for each case with an equation. The slope of the trend line is the coefficient or modulus of horizontal subgrade reaction, k_s, at the ground surface and is also determined along the depth. Non linearity in the relationships is ignored.

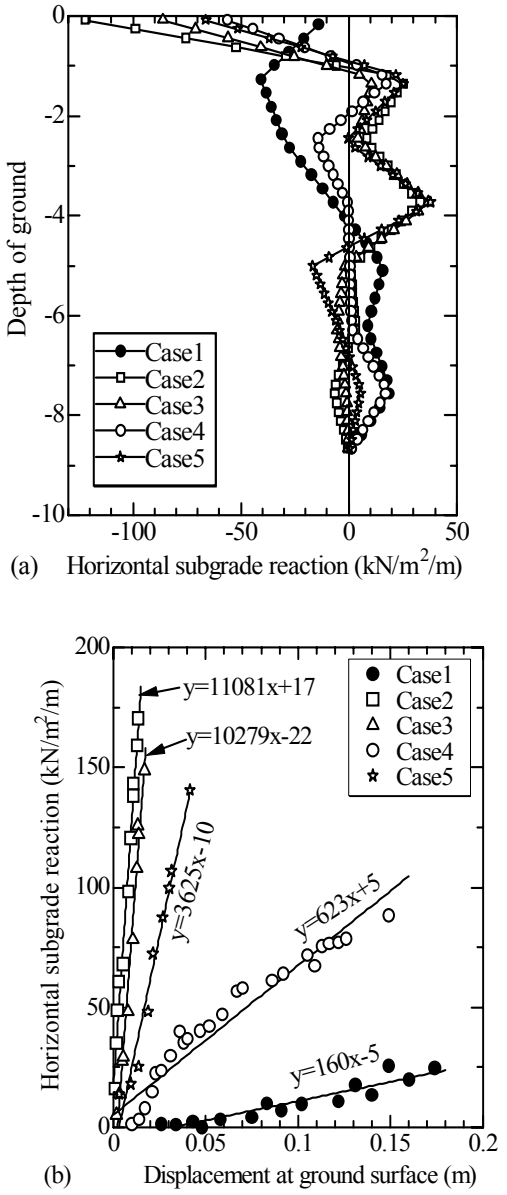

Fig. 18. Determination of horizontal subgrade reaction at the 45 kN/m loading stage: (a) horizontal subgrade reaction along depth, (b) subgrade reaction versus displacement at the ground surface.

Figure 19 shows the variation of the coefficient of horizontal subgrade reaction, k_s, with depth. The resistance from the CDM can be visualized from the figure up to a depth of about 4 m for Cases 3, 4, 5 and 2 m for Cases 6, 7, except for Case 2 with up to about full depth. The value of k_s at ground surface in the improved cases ranges from 625 to 11000 kN/m^3 whereas k_s of the unimproved case is 160 kN/m^3 (**Figs. 18(b)** and **19**). The k_s in the improved zone increases almost linearly.

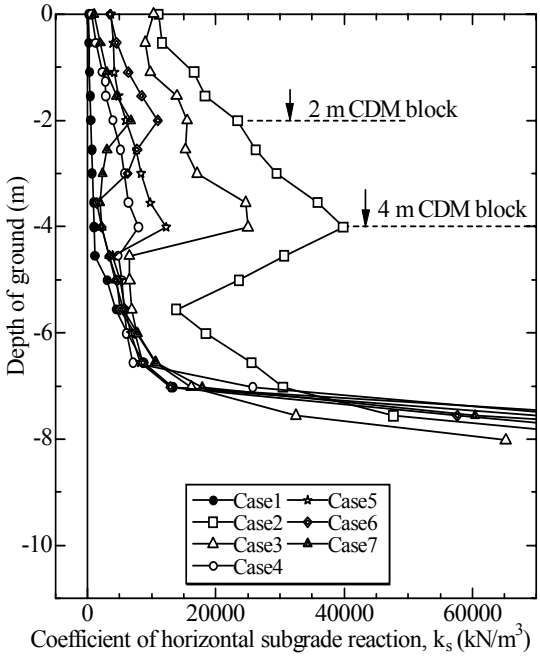

Fig. 19. Coefficient of horizontal subgrade reaction, k_s along depth at the 45 kN/m loading stage.

Shear force and horizontal load distributions derived from the numerical method are shown in **Figs. 20(a)** and **20(b)** respectively. Shear force at ground level is -45 kN/m and below the ground level in some cases it reaches about +60 kN/m. Horizontal distributed load to the quay wall (**Fig. 20(b)**) is a kind of horizontal subgrade reaction which is stated in **Fig. 18(a)**. Maximum distributed load in the unimproved case (Case 1) is obtained as -35 kN/m^2/m (in the test it was -12 kN/m^2/m) and in the improved cases it ranges from -70 kN/m^2/m to -184 kN/m^2/m (in the test it was -60 to -125 kN/m^2/m). Predicted subgrade load-distributions compare fairly well the horizontal subgrade reaction.

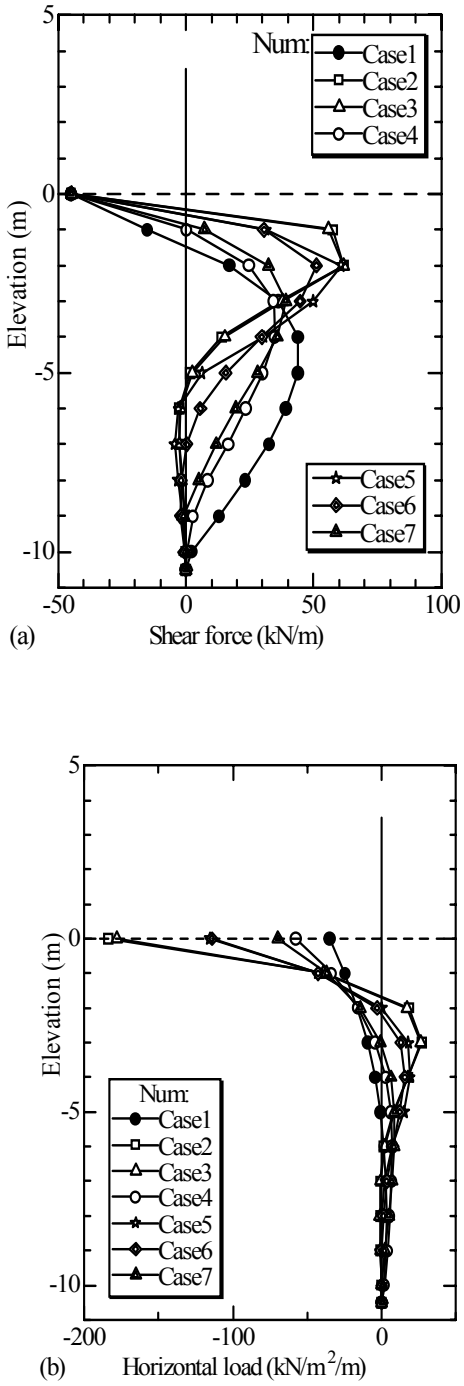

Fig. 20. Shear forces and horizontal load distributions at 45 kN/m loading derived by the numerical method.

(8) Effect of size of the CDM

The effect of width of the CDM on the coefficient of horizontal subgrade reaction, k_s, is shown in **Fig. 21**. For the cases with 4 m depth CDM, the width effect is considered at the depth of 0 m, 2 m and 4 m (**Fig. 21(a)**). Likewise the cases with 2 m depth CDM, the

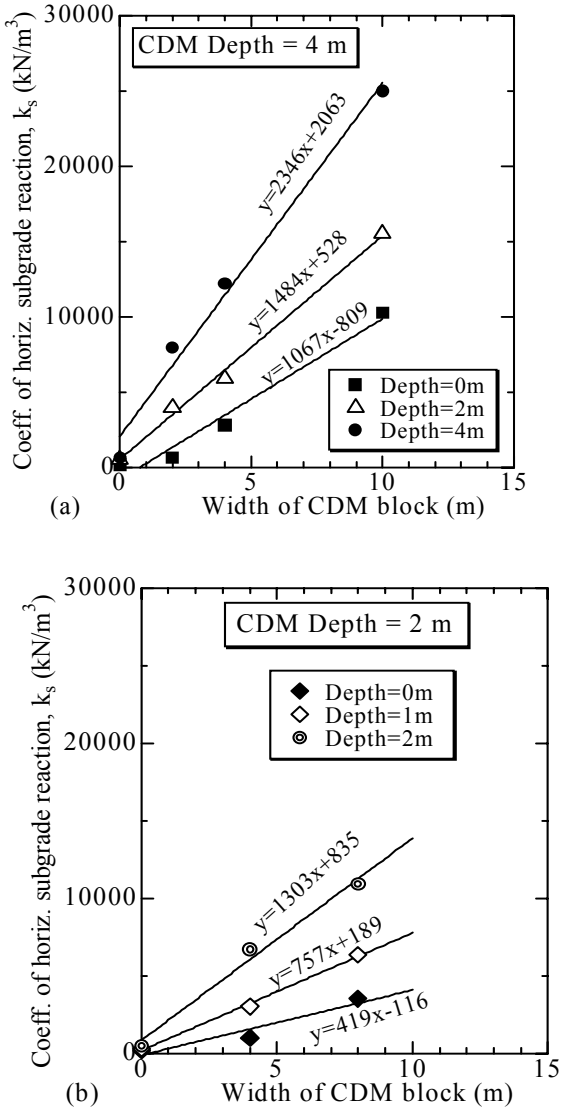

Fig. 21. Variation of coefficient of horizontal subgrade reaction, k_s with the width of CDM block: (a) depth of the CDM block is 4 m and (b) depth of the CDM block is 2 m.

width effect is considered at the depth of 0 m, 1 m and 2 m (**Fig. 21(b)**). With the same depth of CDM, k_s increases almost proportionally with increase in width of the CDM. From the relationship between the k_s and width of the CDM as shown in the figures, k_s corresponding to any other widths are determined and used in the numerical method in the following paragraphs. The relationship of the k_s versus width of the CDM can be produced for any other depths also. Average k_s values used in the numerical calculations along depth is listed in **Table 6**. The k_s can also be obtained from the

Table 6. k_s values used in numerical analysis.

Depth of Ground	Case 1	Case 2	Case 3	Case 4	Case 5	Case 6	Case 7
0 m	160	11,080	10,280	625	3,625	3,510	1,010
2 m	500	23,400	12,000	2,300	4,500	6,700	3,400
4 m	1,050	32,800	21,000	6,300	9,500	4,400	2,400
6 m	6,000	18,400	7,700	5,500	5,400	5,100	5,300
8 m	14,000	30,400	32,500	25,800	13,000	12,900	17,900
10 m	85,200	88,400	65,200	77,200	70,400	57,700	60,400

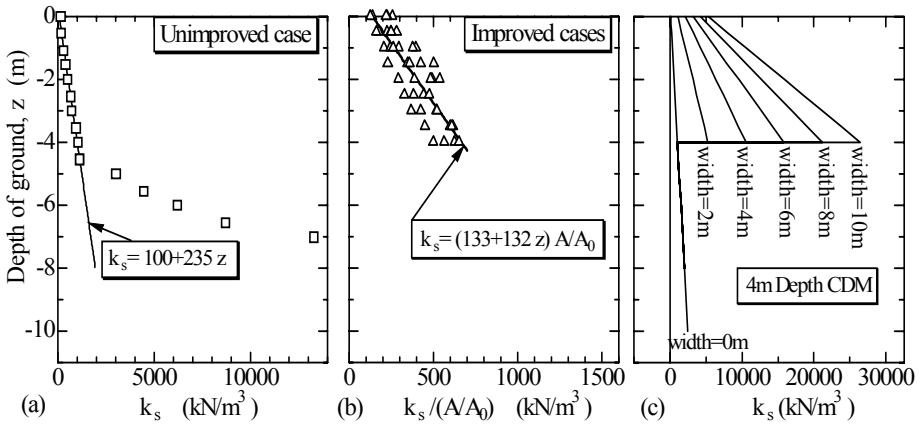

Fig. 22. Simplification of coefficient of horizontal subgrade reaction, k_s: (a) simplified k_s along depth for the unimproved case, (b) k_s normalized by sectional area of the CDM block, A, (A_0 = unit width) along depth and (c) simplified k_s along depth for 4 m depth CDM.

relationships of various parameters like shear modulus, Poisson ratio, shear strength, friction angle, and cohesion along the depth of the ground. Numerically the k_s can be determined by the following model of Bowles (1974).

$$k_s = A_s + B_s z^n \tag{8}$$

where A_s= constant for structural member, B_s= coefficient for depth, z = depth of interest below ground and n= exponent to give k_s the best fit (if load test or other data are available). Bowles (1974) has shown that this model is reasonably correct by using it to analyze full-scale field walls and for reanalyzing model sheet pile walls reported by Tschebotarioff (1949) and by Rowe (1952). To use this model, the CDM zone can be treated either as a layer like soil or a hybrid zone whose property will be obtained by considering the interaction among the sheet pile wall, the CDM and the surrounding clay.

Three different methods to determine the coefficient of horizontal subgrade reaction, k_s are introduced.

I. Simplification with CDM area: This method is described in **Fig. 22**. Largest displacement of the sheet pile quay wall was observed in the unimproved case (Case 1). Since the displacement of the quay wall in the deeper ground is very small, below 6 m depth the k_s values observed in **Fig. 19** (test data) are erroneous. Test data of k_s until about 5 m depth is considered to extrapolate the k_s variation with depth in unimproved case (**Fig. 22(a)**). The relationship derived for the unimproved ground is:

$$k_s = 100 + 235z \tag{9}$$

where z is the depth (m) from the ground level. All of the k_s data of improved cases are normalized by the cross sectional area, A, of the CDM block and plotted against the depth, z (**Fig. 22(b)**). The average trend line gives the following relationship:

k_s=(133+132 z)A (10)

From these two equations (Eq. (9) and (10)) simplified k_s values are produced along the depth and shown in **Fig. 22(c)**. In the figure, simplified k_s values are shown for various width of a 4 m depth CDM block. Below the CDM block, the k_s value is assumed as the value of unimproved case (Eq. (9)).

II. Simplification with CDM width: This method is described in **Fig. 23**. The simplified relationship derived for the unimproved ground is same as described in the first method with Eq. (9). All of the k_s data of improved cases are normalized by the width, W, of the CDM block and plotted against the depth, z (**Fig. 23(b)**). The average trend line gives the following relationship:

k_s=(200+850 z)W (11)

From Eqs. (9) and (11) simplified k_s values are produced along the depth and shown in **Fig. 23(c)**. In the figure, simplified k_s values are shown for various width of a 8 m depth CDM block. Below the CDM block, the k_s value is assumed as the value of unimproved case (Eq. (9)).

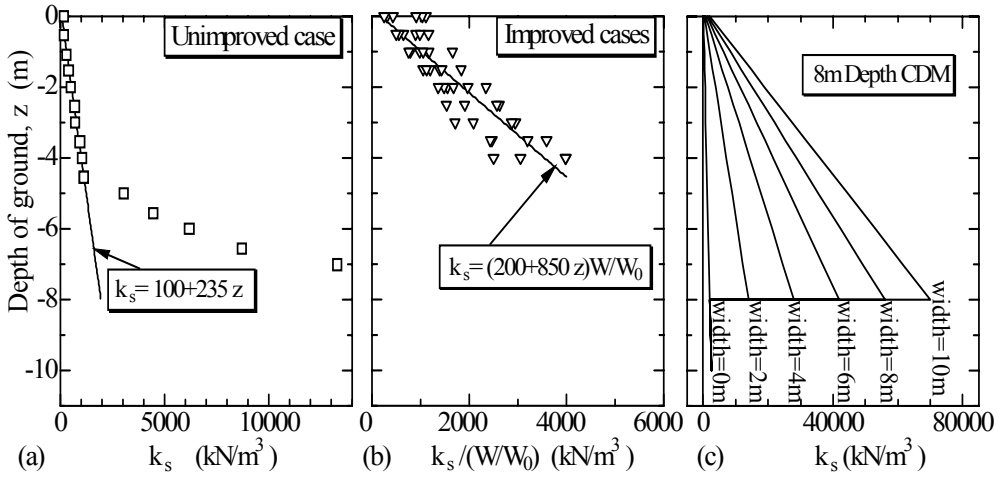

Fig. 23. Simplification of coefficient of horizontal subgrade reaction, k_s: (a) simplified k_s along depth for the unimproved case, (b) k_s normalized by width of the CDM block, W, (W_0 = unit width) along depth and (c) simplified k_s along depth for 8 m depth CDM.

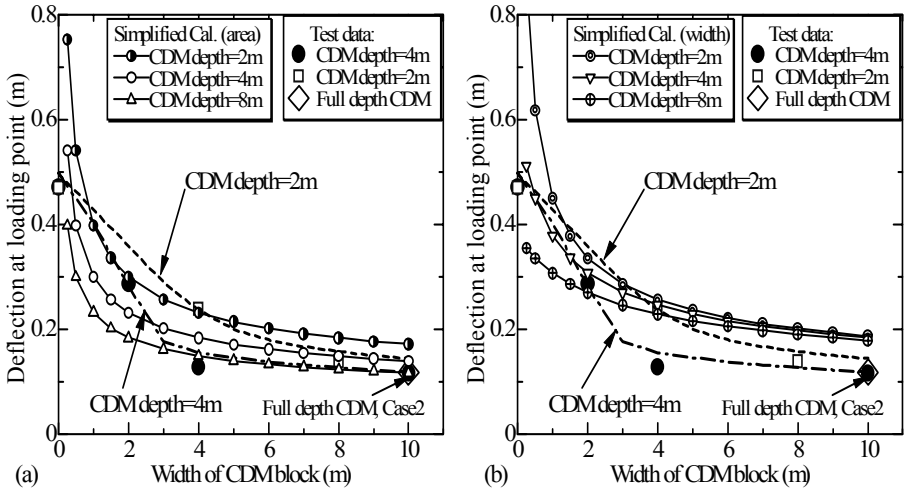

Fig. 24. Effect of the width of CDM block at the 45kN/m loading: (a) simplified calculation with respect to the sectional area of the CDM block and (b) simplified calculation with respect to the width of the CDM block.

III. Centrifuge test data: The k_s value obtained in this method is from the test data (**Table 5**). It is described in **Figs. 18** and **19**. Deflection of the quay wall is obtained numerically for various width and depth of the CDM by using the k_s value. The k_s values are obtained from the above methods. **Figure 24** shows the relationship between deflection at loading point at the 45 kN/m loading stage and the width of the CDM block. Test data and numerical predictions are plotted in the figure. The dash-dotted line indicates the trend for CDM of depth equal to 4 m and the dashed line for CDM of depth equal to 2 m (**Figs. 2**4(a) and **24(b)**). These two lines were calculated by the method- *III*. In the 4 m depth line, increasing the width of CDM block up to about 3 m proportionally reduces the deflection of the quay wall, which then reduces to the lowest deflection quickly.

Deflection presented by the 2 m depth line decreases proportionally up to about 4 m of CDM width and then reduces to the lowest deflection. Test data are also plotted in the figures. Full-depth CDM (Case 2) also falls in the zone of lowest deflection. This figure implied that beyond 4 m width, CDM of 2 m depth is more efficient than that of 4 m depth or full-depth in reducing the deflection of the sheet pile quay wall. Since Cases 2 and 3, which have the same width but different depths (full- and half-depth), show the same deflection, from an economical feasibility point of view half-depth or the floating type CDM is more efficient for the field situation.

Simplified calculation with respect to the CDM area (method- *I*) is shown in **Fig. 24(a)** for the depth of 2 m, 4 m and 8 m. Reasonable predictions are observed throughout width of the CDM. Simplified calculation with respect to the CDM width (method- *II*) is shown in **Fig. 24(b)** for the depth of 2 m, 4 m and 8 m. These three lines show a tendency of merging at 7 m width of the CDM. It means beyond 7 m width, deflection is same for any depth of the CDM and the lowest deflection is about 0.2 m. Numerical prediction with area based simplification (method- *I*) agrees well with the test data and shows better prediction than that of width based simplification (method- *II*).

3.7 Conclusions on *pseudo-static* loaded sheet pile quay wall

The effects of sea-side ground improvement on the stability of existing sheet pile quay walls have been presented with reference to the load-deflection behavior, effect of size of cement deep mixing zone, and wall deflection, bending moment, horizontal subgrade reaction and earth pressure distributions in a series of centrifuge tests. The effects of sea-side ground improvement on the stability of existing sheet pile quay wall also have been numerically predicted. Numerical predictions compare satisfactorily with the centrifuge test results. The method can be used for predicting the important design parameters like deflection, bending moment, shear force and horizontal subgrade reaction or load to the sheet pile quay wall. The conclusions of the pseudo-static study are as follows:

1. Compared with the case of a wall embedded in unimproved ground, significant resistance against cyclic horizontal load was observed to develop in the CDM improved cases, i.e. the horizontal deflection was effectively reduced.
2. The horizontal deflection of the model quay wall decreased proportionally with increase in width of the CDM area until it reaches a certain limit.
3. In the cases of improved ground, the maximum bending moment of the model quay wall was reduced up to about half of the value of the unimproved ground case.
4. The horizontal load was mainly resisted by the improved soil zone, which offered large horizontal subgrade reactions.
5. Seaward rotational tendency of the CDM block was observed in the improved ground cases.
6. Proposed numerical model of the sheet pile quay wall can predict the effect of the sea-side ground improvement.
7. Prediction by the numerical model agrees fairly well with the results of centrifuge model tests.

4. Dynamic Loaded Sheet Pile Quay Wall

4.1 Model set-up

Figure 25 shows the schematic illustration of the model set-up. A strong box of 735 mm length, 500 mm depth and 200 mm breadth with a transparent front window was used for the tests. Wave absorbing materials were set on 200 mm faces of the strong box. Photos of model set-up are shown in **Fig. 26**. The model sheet pile quay wall is a 3 mm thick steel plate instrumented with 7 pair of strain gauges (S1 to S7) and 15 earth pressure gauges (E1 to E14 and E56) on both sides. At the bottom of the strong box, the sheet pile wall is set on a 10 mm thick rough surfaced acrylic plate and at the top it is clamped with guide plates, so that it is firmly fixed and remains vertical during the model preparation. The flexural rigidity, EI, of the prototype sheet pile wall is 5.65×104 kN.m^2/m. Prototype section of this plate becomes the Japanese standard sheet pile of type SP-IV (Nippon Steel Corp., 1998).

The model ground is prepared by same manner as the static loading test case (**Fig. 2**).

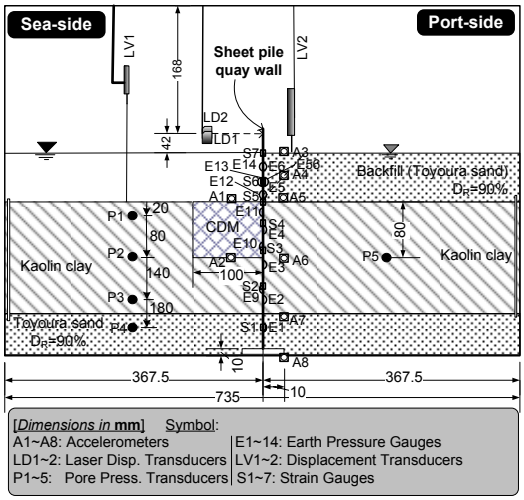

Fig. 25. Model set-up of Case D2 in model scale.

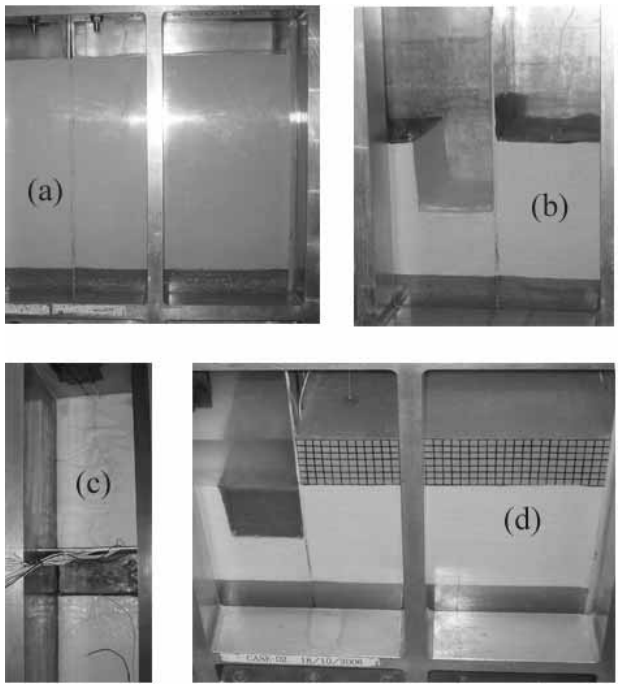

Fig. 26. Construction stages photographs: (a) kaolin clay slurry is poured until the top of the strong box, (b) CDM hole is excavated in the consolidated clay, (c) top view of the model showing the CDM, sheet pile wall and white kaolin, and (d) final model with backfill sand and sea-side water.

Table 7. Dynamic Test Conditions in Prototype scale.

Test Cases	D2	D3	D4	D5
Clay depth (m)	8	8	8	8
CDM zone (m^2)	5×4	0×0	10×8	10×4
Input Acceleration (Gal)	45, 196, 294, 343	30, 118, 226, 322	28, 114, 196, 294, 335	28, 100, 215, 315, 335
No. of shaking	4	4	5	5
q_u of CDM (kPa)	1340	-	580	990

4.2 Test procedures and conditions

(1) Test procedures

The strong box with the model is mounted on the swinging platform of the centrifuge. Centrifugal acceleration is increased up to 50 *g*. At 50 *g*, the bottom sand layer becomes 3 m, clay depth becomes 8 m, backfill and sea water heights become 3.5 m and the prototype CDM areas are shown in **Table 7**. The consolidation in the centrifuge at 50 *g* is conducted until the degree of

consolidation is estimated to have achieved 90%. Data from the pore pressure transducers in the clay and LV1-2 are used to estimate the degree of consolidation. At 50 g, four to five shaking are applied to this model in flight. The shaking is applied parallel to the long side of the strong box. The test conditions in the prototype scale are shown in **Table 7**. Four shakings are applied in Cases D2 and D3 and fives are applied in Cases D4 and D5. The frequency of all shaking is maintained as 2 Hz (100 Hz in model scale) and conducted in 50 sinusoidal cycles. Magnitudes of shaking and other test conditions are listed in **Table 7**. A total of 24 to 30 days (14 to 18 minutes in model scale) are allowed between the shakings to dissipate excess pore water pressure.

Deflection of sheet pile quay wall, pore water pressures in the ground, earth pressures at various elevations and strains on the surface of the sheet pile wall are monitored during the test. The positions of the sensors are shown in **Fig. 25**. Still pictures of the model are taken before and after the each shaking. All the test results in the following sections are presented in the prototype scale.

(2) Test conditions

In this paper, the results of 4 centrifuge tests (Cases D2 to D5) are presented to discuss the effects of the sea-side ground improvement on the stability of the quay wall in seismic loading. All of the test cases are identical except for the size of the CDM block and the position of accelerometer below the CDM. Stability of unimproved and improved sea-side ground has been examined from the unimproved case (Case D3) and the improved cases. The effect of width of the CDM block is investigated from Cases D2 and D5, which have the depth of CDM equal to 4 m. Having the same width of CDM, the influence of the 'floating type' and full-depth CDM is likewise examined from Cases D4 and D5. Cross-sectional area of CDM block in Cases D2, D4 and D5 is different. Sectional-area wise performance has been investigated. All the test results in the following sections are presented in the prototype scale.

4.3 Stress-strength profile of clay stratum

The seashore consists of a thick clay layer underlain by a sand layer. Overconsolidated clay is chosen to facilitate the model preparation. The maximum effective past pressure experienced by the clay can be assumed to be the same as that applied to consolidate the clay, i.e. 150 kPa. Two saturated specimens of Toyoura sand were tested in drained triaxial compression test (JGS 2000, relative density: 80%; σ_3': 100- 200 kPa; σ_1': 500- 760 kPa) and three kaolin clay specimens were tested in undrained triaxial compression tests (JGS 2000, σ_3': 20- 72 kPa; σ_1': 80- 235 kPa) to obtain the critical state parameters of sand and clay. Here σ_3' and σ_1' are effective lateral and vertical stress respectively. The sheet pile was set-up to a certain depth into the strata of sand underlying the clay to ensure firm fixity of the quay wall. Stress history of the clay layer is shown in **Fig. 27**. In the figure, σ_v' and σ_p' are the current effective vertical stress and the past maximum vertical consolidation pressure respectively; *OCR* is the overconsolidation ratio (σ_p'/σ_v'); the coefficient of in-situ earth pressure, K_0, was derived for overconsolidated (OC) clay with a critical state friction angle ϕ=28.6^0, following Eq. (1). The undrained shear

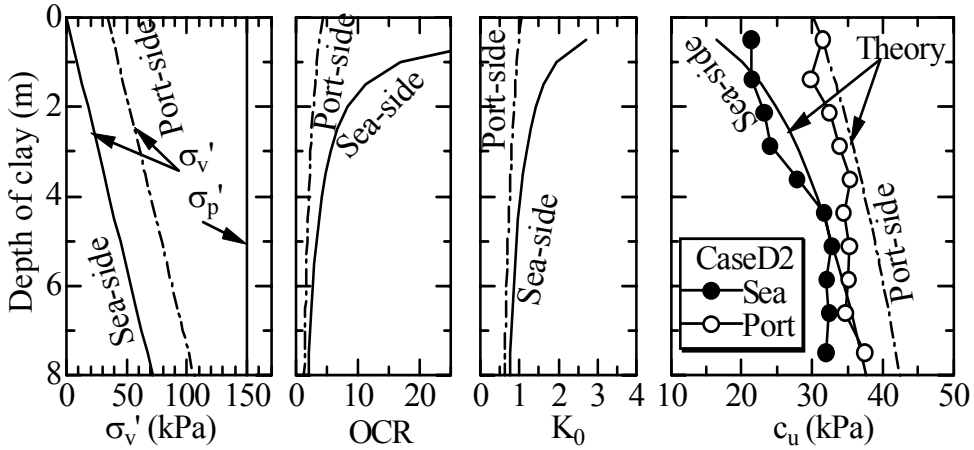

Fig. 27. Stress history and undrained shear strength of the clay stratum.

strength, c_u, of the clay was derived from Eq. (2).

Theoretical c_u values are compared with the test results. The c_u values are computed from the water content profile along the depth both in the sea-side and port-side. After stopping the centrifuge, a few hours have passed before sampling for water content. Some swelling may have taken place in this period, which may result in smaller c_u values than those predicted by theory. The c_u profile of Case D2 is shown in the figure. Although the clay samples are excavated after the test, the values derived from the test results compared fairly well with the theoretical c_u values (**Fig. 27**), which were predicted before the loading stage.

4.4 Results and discussions

(1) Centrifuge consolidation and pore pressures

Data from the pore pressure transducers, P1-5, and displacement transducers, LV1-2 on the clay are used to estimate the degree of consolidation at 50 g prior to the loading stage. Square root of time method was used to estimate the degree of consolidation. Time taken to achieve 90% consolidation in the centrifuge is about 5 hours. Since the depth of the clay stratum in all cases is the same (8 m), almost the same amount of consolidation settlement was observed. This highly overconsolidated clay stratum is found to settle about 0.40 m in the prototype scale. The consolidation process makes the soil a competent foundation with definite stress history. Excess pore pressure in the ground may affect the stability of the sheet pile quay wall significantly. Almost constant equilibrium pore pressure from each of the pore pressure transducers was observed during the loading stage.

(2) Deflection of sheet pile quay wall

Deflection of the quay wall is the main index in describing stability. **Figures 28(a)** to **28(d)** show the in-flight photos of Cases D2, D3, D4 and D5 respectively at the final stage of shaking. Deflection of the sheet pile wall from the vertical position, size and position of the CDM and subsidence of the backfill sand can be seen in the photos.

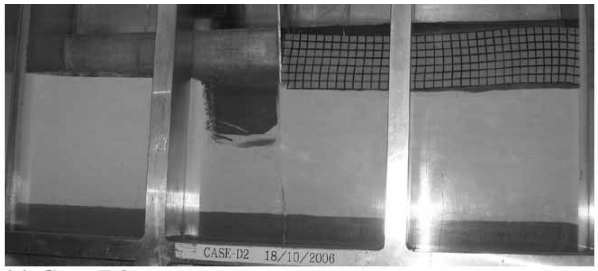

(a) Case D2

(b) Case D3

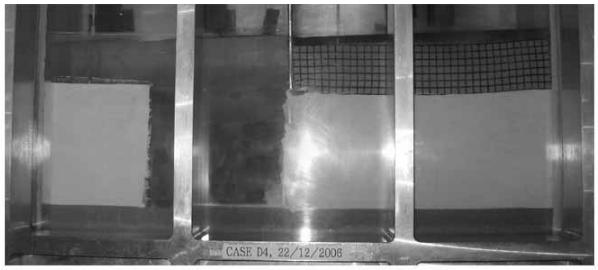

(c) Case D4

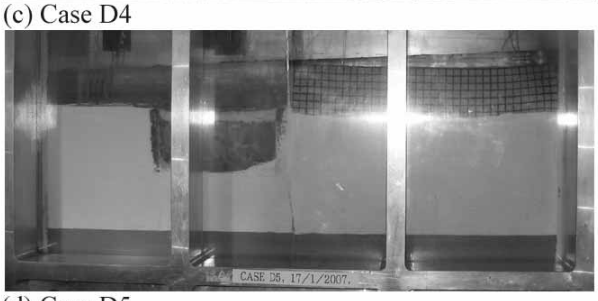

(d) Case D5

Fig. 28. In-flight photo of the sheet pile quay wall of: (a) Case D2 at 343 Gal, (b) Case D3 at 322 Gal, (c) Case D4 at 3335 Gal and (d) Case D5 at 335 Gal, shaking stage.

Figure 29 shows the horizontal deflection - time history of the quay wall at backfill surface level in different stages of shakings. In the first two shakings the quay wall shows larger stiffness and less deflection. In the subsequent shakings Cases D2 and D3 show much more deflections than that of Cases D4 and D5.

The relationship between the horizontal deflection of the quay wall, δ, and input acceleration is shown in **Fig. 30**. Deflection at static mode, δ_s, and final stage of shaking,. δ_f, are tabulated in the figure. Case D3 is

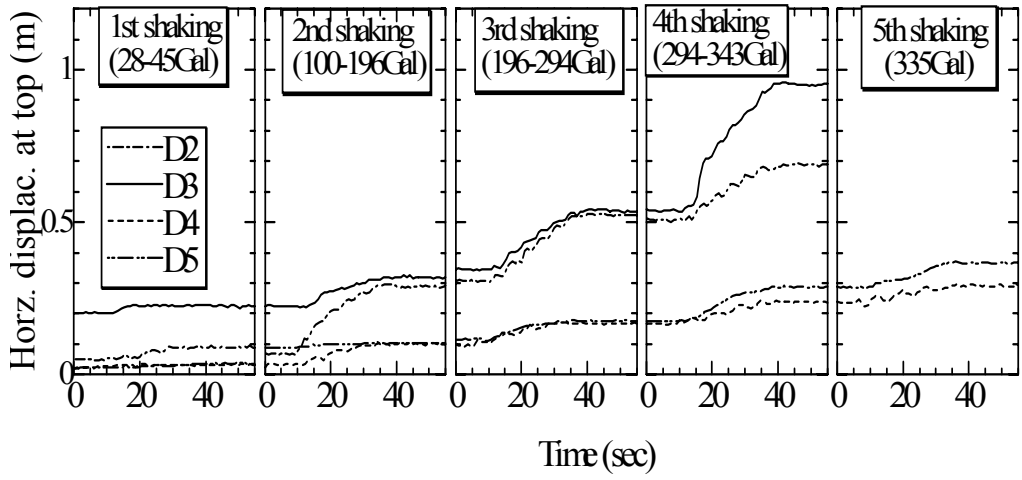

Fig. 29. Horizontal deflection-time history of quay wall at backfill surface level.

without improvement and greatly affected by both the static and seismic loadings. Before the seismic loading the sheet pile is deflected (δ_s) about 0.20 m due to the static loads and the remaining 0.75 m of deflection takes place due to the seismic loads. It is observed that the CDM zone reinforces the stability of the ground significantly. And the improved cases show more stiffness than the unimproved ground case. Static deflection of the unimproved case is 4 to 10 times larger than that of CDM improved cases.

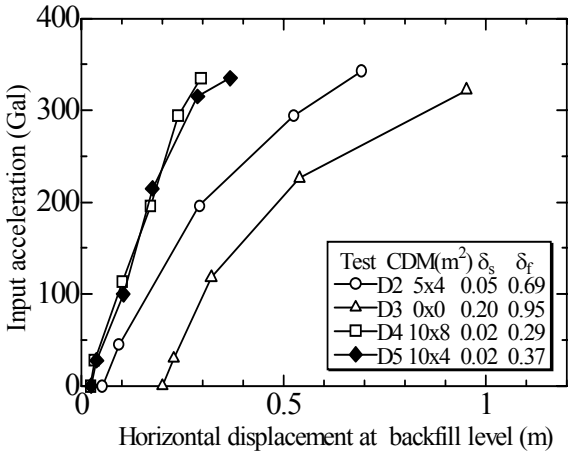

Fig. 30. Horizontal deflection of quay wall at backfill surface level versus input acceleration.

Deflection δ_f of the unimproved Case D3 is 0.95 m whereas full-depth CDM improved ground of Case D4 is 0.29 m. Improved stiffness becomes more than three times larger than that of the unimproved sea-side ground. Here stiffness is indicated as horizontal load per unit deflection. Cases D2 and D5 with the same depth of CDM (depth: 4 m) but different width (respective widths: 5 m and 10 m) have δ_f of 0.69 m and 0.37 m respectively. Here the deflection increases proportionally with the decrease of width of the CDM. In other word, the stiffness offered by the quay wall in these cases is almost proportional with the width of CDM. However, the interaction between the quay wall and the CDM, and between the CDM and the surrounding clay are not yet thoroughly investigated. These interaction processes can affect the deflection of the quay wall significantly. Cases D4 and D5 having full-depth and floating or half-depth CDM (with the same width of treated material) have δ_f value of 0.29 m and 0.37 m respectively. Sectional-area wise performance of the CDM can be compared from Cases D2, D5 and D4. Case D2 having the cross sectional-area, A = 20 m^2 shows δ_f value of 0.69 m, Case D5 having A = 40 m^2 shows δ_f value of 0.37 m and Case D4 having A = 80 m^2 shows δ_f value of 0.29 m. Although the stiffness is sensitive in smaller area cases, increasing the width or size of the CDM to the full depth of the clay results a small amount of deflection of the quay wall.

This study implies that the final deflection of the unimproved case is almost 3.25 times larger than that of full-depth CDM case; 2.5 times larger than that of half-depth CDM case and 1.4 times larger than that of smallest-size CDM case. The smaller width CDM case (Case D2) shows the deflection about double than that of Case D5. On the other hand Case D5 shows the deflection almost same as the deflection of the full depth

CDM case. From an economical feasibility point of view the half-depth or the floating type CDM with larger width can be recommended for the field.

(3) Excess pore water pressure

Although a pore fluid with viscosity of 50 times that of water would be necessary to satisfy the scaling laws (at 50 *g*) as discussed in the previous section, tap water is used to saturate the backfill and to fill the sea-side, thus increasing the rate of dissipation of excess pore water pressure by a factor of 50. Excess pore water pressure ratio is computed by dividing the generated excess pore water pressure by the initial effective overburden stress. **Figure 31** shows the time histories of the excess pore water pressure ratio in the sea-side and port-side during all of the shakings. Pore pressure transducers, P1 to P4 are set from the top of the clay to the bottom of sand layer (**Fig. 25**). The excess pore water pressure ratio quickly rises to the peak soon after the start of shaking and gradually dissipates with time. Maximum pore pressure ratios observed in Cases D2, D3, D4 and D5 are 0.62, 0.57, 0.72 and 0.71 respectively. These maximum pressure ratios are recorded from the top most pore pressure transducers (P1). It is observed by Takahashi et al. (2006) that the ground liquefies at the shallow depth first and liquefaction occurs in the entire ground with increasing the magnitude of excitation. It can be seen from the plots that after each shaking some amount of residual excess pore water pressures remain in the ground. This residual pressure may affect the stiffness of the ground during other seismic motion. During the shaking with larger acceleration the residual pressure can weaken the shear stress transmission inside the ground. However, only one step shaking test with the same acceleration could produce different behavior of the sheet pile quay wall.

(4) Acceleration time histories

As shown in **Fig. 25**, accelerations were recorded at various points throughout the model. **Figures 32** and **33** illustrate the excitation-time histories recorded in 45 Gal, 196 Gal and 343 Gal shakings of Case D2 in the sea-side and port-side respectively. These two figures also compare the excitation histories in the improved sea-side and port-side. At 45 Gal shaking it is apparent that the motion is significantly thickened from the bottom of the clay layer to the top of the backfill sand. Accelerometers A1 and A2 (CDM zone) were placed

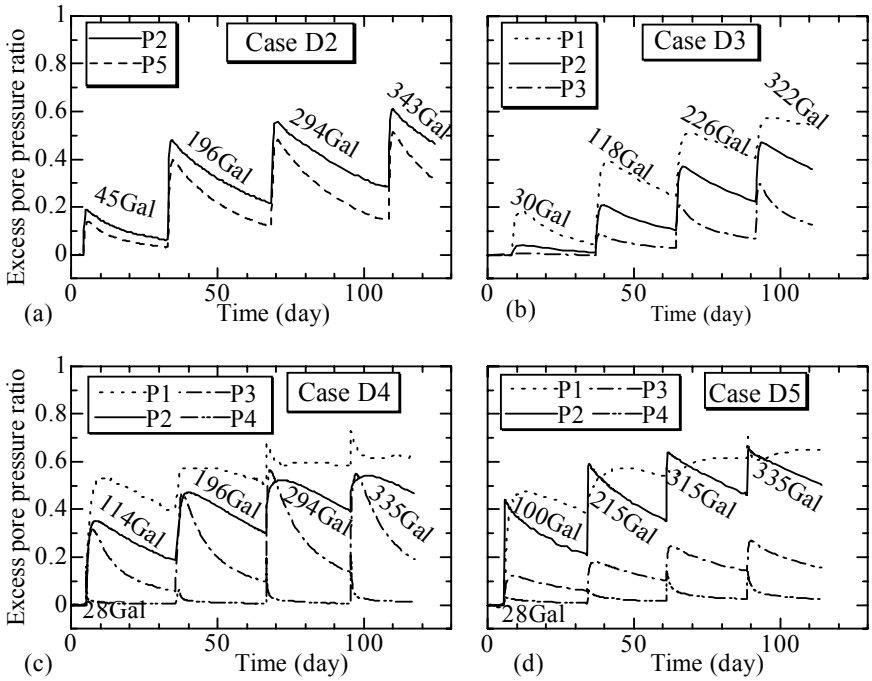

Fig. 31. Excess pore water pressure during the seismic loading in: (a) Case D2, (b) Case D3, (c) Case D4 and (d) Case D5.

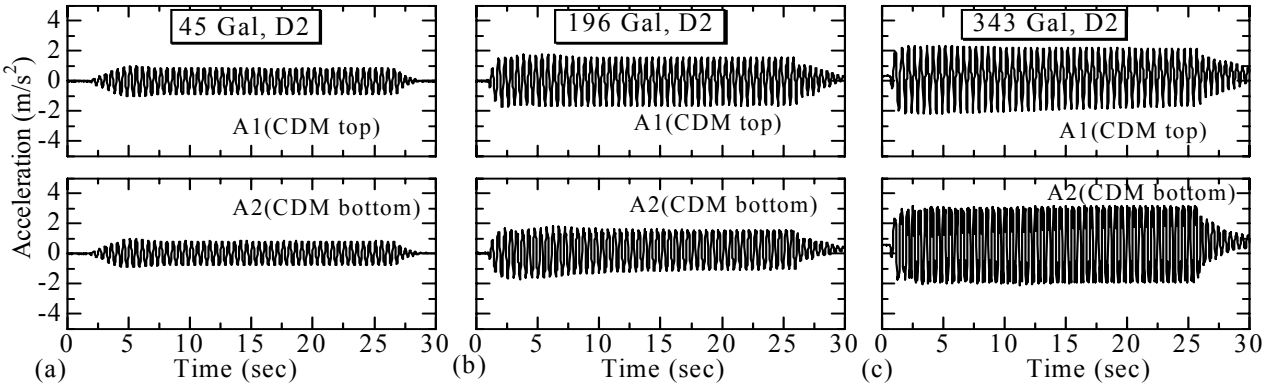

Fig. 32. Acceleration time histories at top and bottom of CDM of Case D2 for: (a) 45 Gal, (b) 196 Gal and (c) 343 Gal shaking.

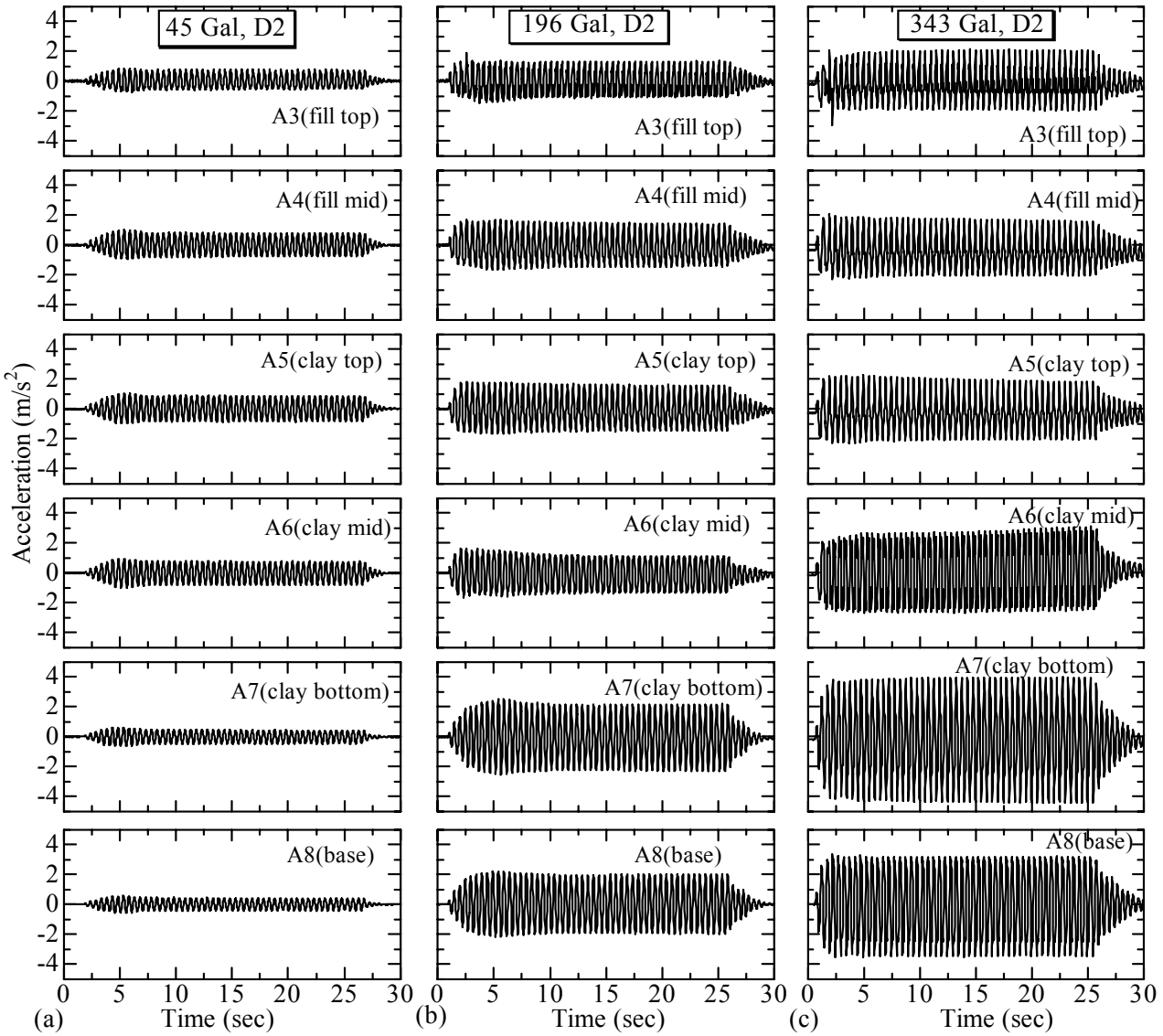

Fig. 33. Acceleration time histories in the port-side ground of Case D2 for: (a) 45 Gal, (b) 196 Gal and (c) 343 Gal shaking.

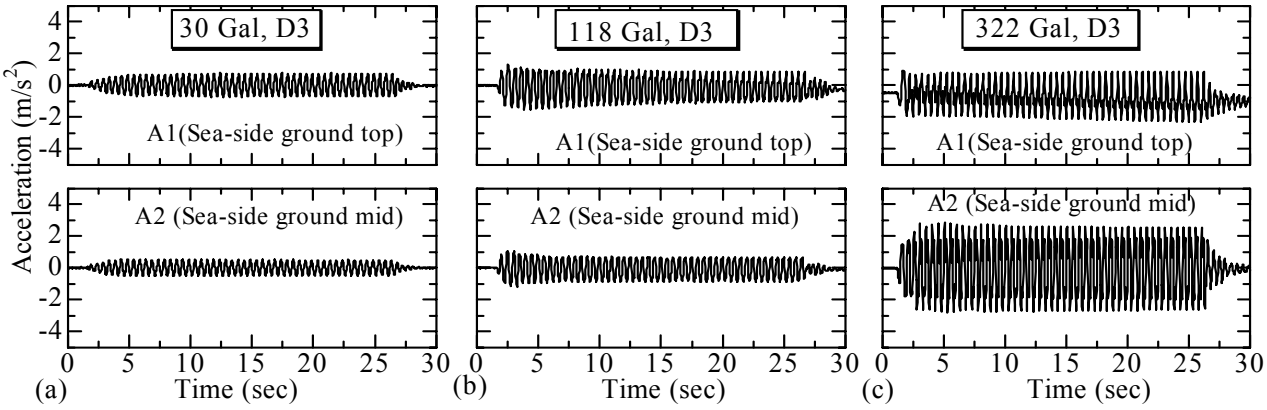

Fig. 34. Acceleration time histories at sea-side ground top and mid of Case D3 for: (a) 30 Gal, (b) 118 Gal and (c) 322 Gal shaking.

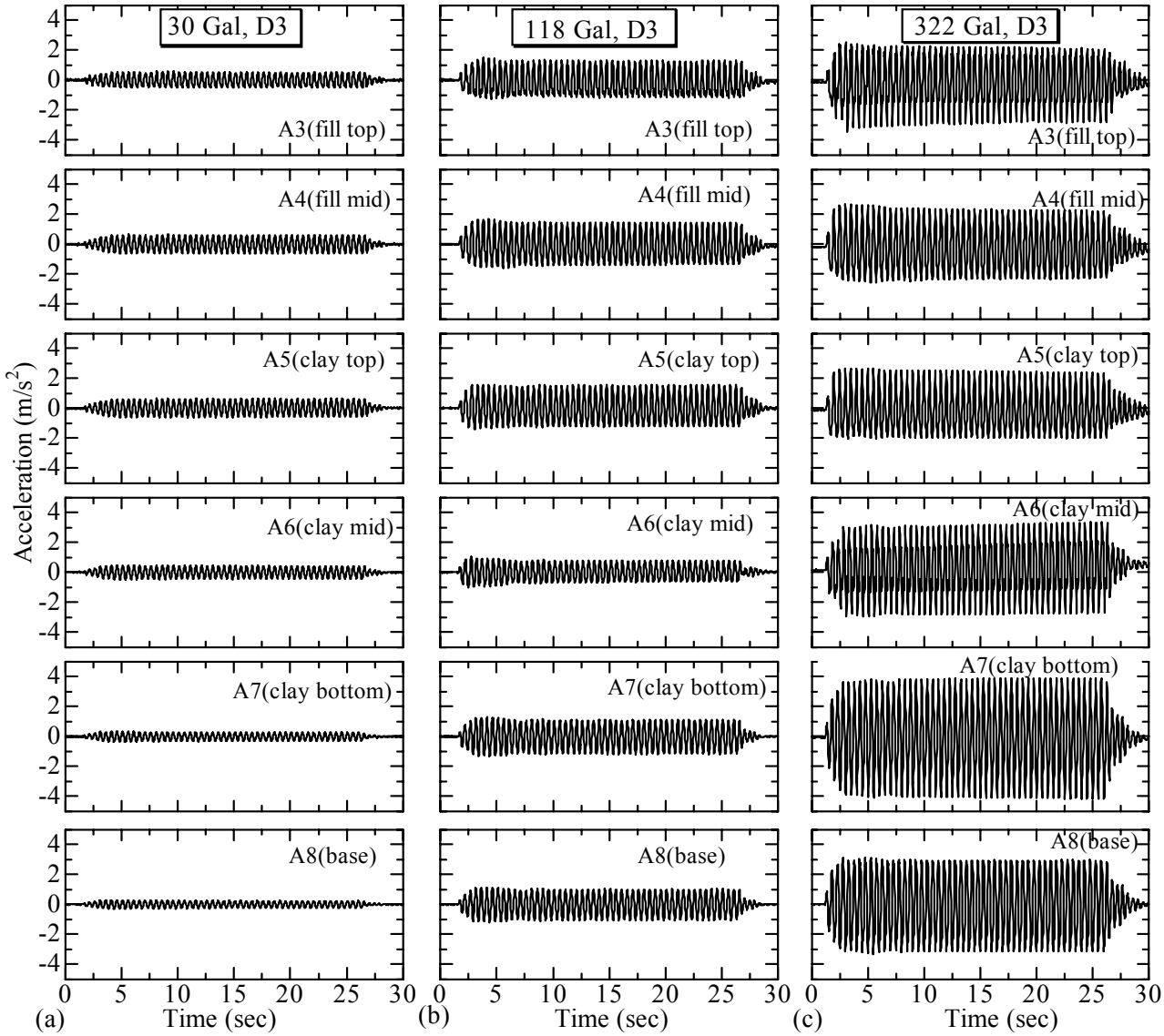

Fig. 35. Acceleration time histories in the port-side ground of Case D3 for: (a) 30 Gal, (b) 118 Gal and (c) 322 Gal shaking.

almost at the same level as A5 and A6 (port-side clay). It can be seen from **Figs. 32(a)** and **33(a)** that the acceleration histories in A1, A2 and A5, A6 are almost similar in the first stage of shaking. Initially the clay, CDM and sand layers were well integrated. The initial stiffness of the sheet pile quay wall system was larger and different in the subsequent loading stages, so that the motion in 343 Gal stage is different and weakened from the bottom of the clay to the top of the backfill sand. In 196 Gal shaking stage (**Figs. 32(b)** and **33(b)**), the base, clay bottom and CDM top felt relatively strong motion.

Figures 34 and **35** illustrate the excitation-time histories of unimproved case (Case D3) in the sea-side and port-side respectively. Locations of A1 and A2 in the sea-side clay were same as the depth of A5 and A6. Locations of the all accelerometers in the Cases D2 and D3 are identical. Although in the first shaking (30 Gal, **Figs. 34(a)** and **35(a)**) the magnitude of accelerations is smaller than that of Case D2, the motion is significantly thickened from the bottom of the clay layer to the top of backfill sand or top of the clay in the sea-side. In the 118 Gal shaking stage (**Figs. 34(b)** and **35(c)**), the motion is still thickening from the bottom of the clay to the top of the backfill sand or top of the clay in the sea-side except for the clay mid in the port-side. Weakening of the motion from the bottom of the clay to the top of the backfill sand or clay in the sea-side is observed in the final shaking (322 Gal, **Figs. 34(c)** and **35(c)**). The similar behavior of propagation of accelerations is also observed in other cases.

The maximum accelerations measured at various depth of the ground during the first and final shakings are plotted in **Fig. 36**. Maximum accelerations of all test cases are shown in the figure. Initially the rising trends of acceleration are found from the bottom of the clay to the top of the sand fill, though constant acceleration is seen in the bottom sand layer. The trend in the final shaking is different from the initial one. Almost increasing trends in the bottom sand layer and decreasing trends from the bottom of the clay to the top of the fill sand are found in the final stage of shaking. Behavior of Case D4 in the final stage is little exceptional to the others. It could be due the stiffness provided by the CDM until the bottom sand layer. Similar effect is also observed in Case D5 which has the half-depth CDM of largest width.

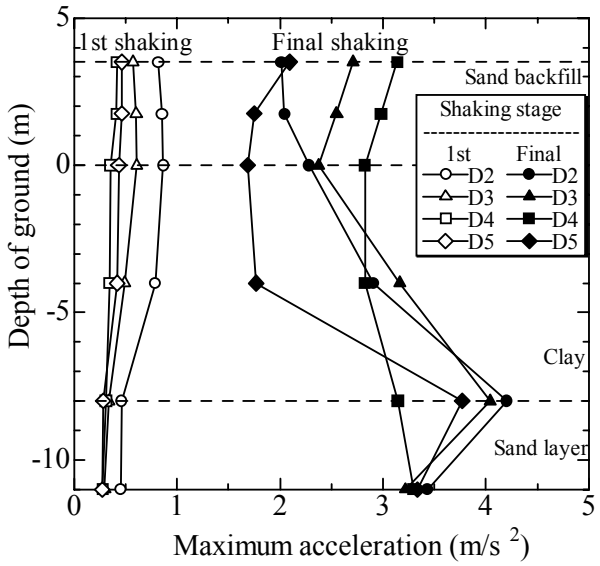

Fig. 36. Propagation of maximum acceleration along the depth of the ground.

Figures 37 and **38** show the time lag in acceleration waves in the port-side and sea-side of Case D2 respectively. Acceleration in the port-side is considered at the clay-bottom (A7), the clay-mid (A6), the clay-top (A5) and the backfill top (A3). In the sea-side acceleration is considered at the clay-bottom (A7), the CDM-bottom (A2) and the CDM-top (A1). The figures are produced from the final phases of acceleration-time histories that presented in **Figs. 32** and **33**. Time lags compare to bottom accelerometer (A7) are shown in the figures and marked as Δ_{71}, Δ_{72} in the sea-side and Δ_{73}, Δ_{75}, Δ_{76} in the port-side. Suffix 71, 72 etc. indicates the lagging between A7 and A1; A7 and A2 respectively. Time lags are calculated from difference among maximum accelerations in the same phase.

It can be seen in **Fig. 37(a)** that time lag in 45 Gal shaking is smaller than that in other shakings. The values of Δ_{73}, Δ_{75}, Δ_{76} in higher excitations (**Figs. 37(b)**, to **37(d)**) are almost same. Value of Δ_{73} is about 0.25s, Δ_{75} is about 0.20s, Δ_{76} is about 0.13s. Time lag at sea-side in 45 Gal shaking is also found smaller than that in other shakings **Fig. 3**8(a). The values of Δ_{71} and Δ_{72} in higher excitations (**Figs. 38(b)** to **38(d)**) are almost same. Value of Δ_{71} ranges between 0.20s to 0.23s, Δ_{72} ranges between 0.10s to 0.12s.

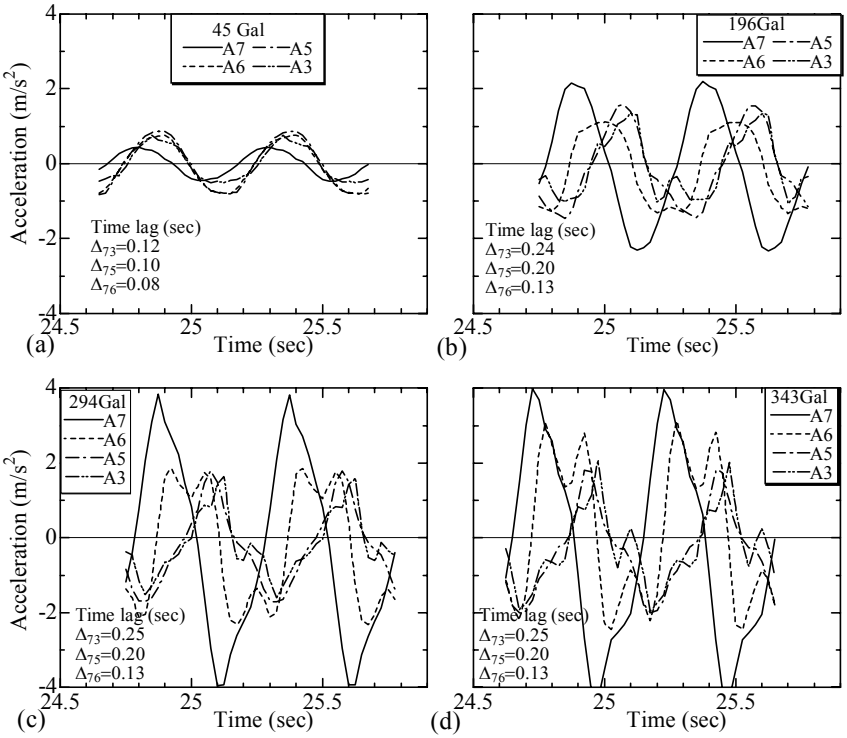

Fig. 37. Acceleration time lag in the port-side of Case D2.

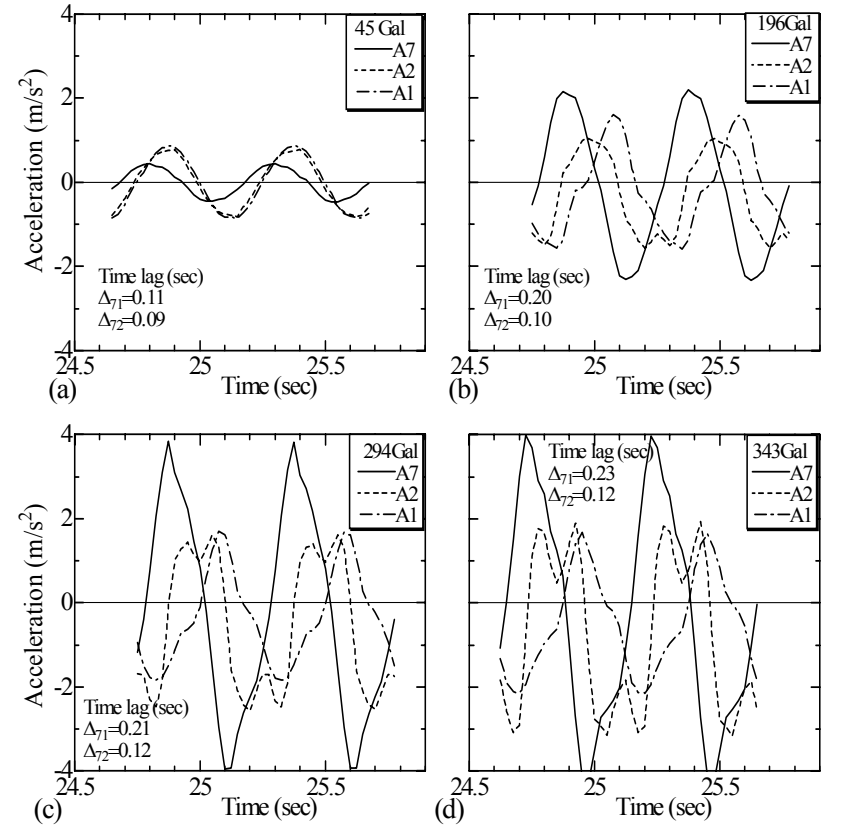

Fig. 38. Acceleration time lag in the sea-side of Case D2.

In the first two shakings the shape of the waves remains almost sinusoidal but during the last two shakings spiky accelerations are observed in both sides. The initial stiffness of the system may be diminished by successive intense earthquake loading. However, limitation of the shaking table in large input acceleration produces the spiky waves.

Calculated time lag versus depth of ground is plotted in **Fig. 39**. Profile in the sea-side is shown with dashed line and in port-side with solid line. At 45 Gal shaking there is clear difference of time lag between sea-side and port-side along depth. In higher excitation both sides also exhibit very little to negligible time difference along the depth.

(5) Earth pressures

Horizontal earth pressures are measured with the earth pressure gauges installed on the sheet pile wall (**Fig. 25**). **Figure 40** shows the horizontal earth pressure both in the sea-side and port-side at initial and final shaking. Data is collected as the maximum value of last phases of the final shaking. Calculated active and passive earth pressures in both the static mode and dynamic mode (k_h = 0.25, Okabe, 1924 method) are also

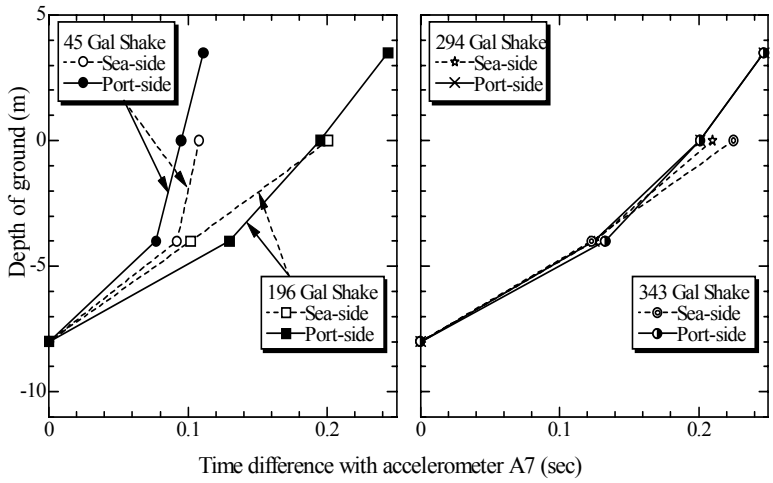

Fig. 39. Comparison of acceleration time lag in both the port-side and sea-side of Case D2.

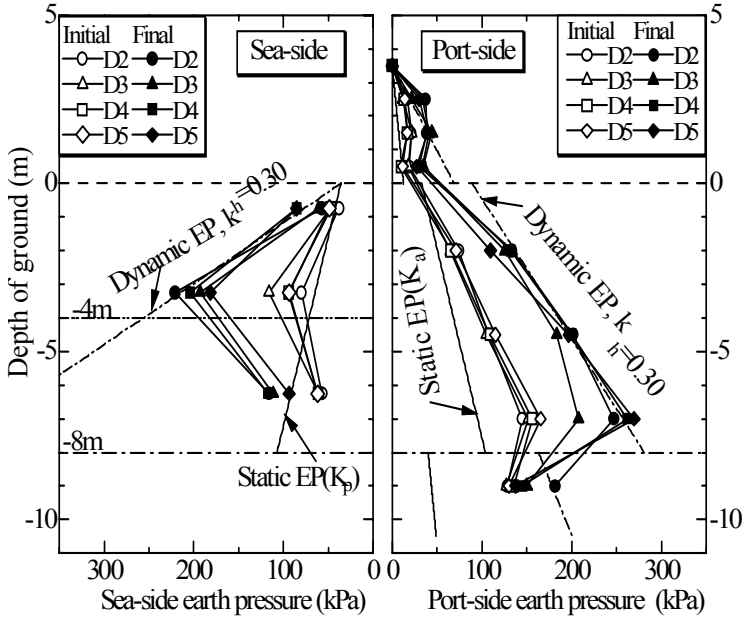

Fig. 40. Lateral earth pressure on the sheet pile quay wall.

plotted in the figure. In the figure, K_a and K_p indicate the theoretical earth pressure coefficient at the active and passive state respectively. Initial earth pressures data are taken from the end of the in-flight consolidation. Reasonable initial earth pressure profile is observed in the figure. Average horizontal seismic coefficient, k_h equal to 0.25 is considered in calculating the dynamic earth pressures. Earth pressure in the backfill (port-side) shows nonlinear variation. The dynamic active earth pressure increases consistently with the increases of acceleration. Similar relationship is observed in all cases during the shaking. Due to the bottom sand layer, pressure has a decreasing trend. Trend of horizontal earth pressure in the sea-side is different from the port-side. The top two sensors (E11 and E10) are inside the CDM block in all improved cases. It is seen from the figure that the middle sensor (E10) experiences larger pressure. Shorter drainage path to the top (E11) and bottom earth pressure gauge (E9) can affect such pressure profile. However the earth pressure profile in the sea-side is quite reasonable. Calculated earth pressure lines agree fairly well with the test data.

(6) Bending moments and structural deflection

Bending moments are derived from the responses of the strain gauges (S) along the sheet pile wall (**Fig. 25**). **Figure 41(a)** shows the bending moment of the sheet pile quay wall at the final stage of shaking. Maximum bending moment is observed at about the mid of the clay ground, whereas in the *pseudo-static* studies (Section 3.6 (6)) maximum bending moments took place at the ground level. The maximum bending moment observed in the unimproved case (Case D3) is about 900 kN-m and in the improved cases (D2, D5 and D4) are 660, 430 and 360 kN-m. This data imply that ground improvement can reduce 30% to 60% bending moment during seismic loading. Interaction among the CDM, the sheet pile wall and the clay reduces the bending moments according to the size of the CDM block. Although the CDM block in the sea-side is relatively stiffer than the port-side clay, the dynamic active earth pressure from the backfill and the clay is much larger than the resistance by the CDM. Due to firm fixation by the bottom dense sand and mobilized active pressures, the sheet pile wall starts to bend at bottom of the clay layer (**Fig. 28**). Seaward rotational movement of the CDM block is also observed in the smallest size CDM case (Case D2).

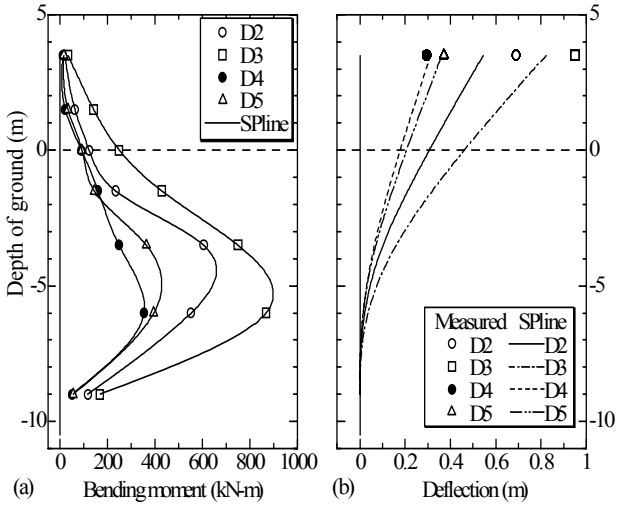

Fig. 41. Bending moment and deflection distribution of quay wall.

Quantic spline functions are used to fit the measured bending moment distribution. The marks in the bending moment curve (**Fig. 41 (a)**) are test data and the curve itself from spline equations. Two successive integrations of this curve lead to the determination of the lateral deflection along the wall, which is shown in **Fig. 41(b)**. Since the subgrade reaction geometrically represents the curvature of the bending moment distribution, it is very sensitive to any fluctuation of the bending moment at a given depth and therefore strongly depends on the choice of the fitting curve of the bending moment (King, 1994). Although the trends from spline equations are seen as slightly irregular, it should be smooth nonlinear curves. From the deflection distribution of the sheet pile quay wall firm fixity at the bottom part, the gradual bending at the clay bottom and the maximum displacement at the top can be visualized. Test data of deflection at the final shaking is also plotted in the graph and agrees well with the plot of deflection distribution.

(7) Effect of size of CDM

Deflection of the quay wall is obtained with the proposed numerical method (Section 3.5) for various cross sectional area of CDM by using the k_s value. The k_s values are obtained from Eqs. (9) and (10) (Section 3.6 (8)) and using the parameters shown in **Table 8**. **Figure 42** shows the relationship between the deflection at top at the static and final stage of shaking and the area of CDM block. Test data and numerical predictions are plotted in the figure. Marks are the test data and the lines are the numerical prediction. Static and dynamic final stage deflection data are also tabulated in **Fig. 30**. The dash-dotted line indicates the trend for static loading condition and the solid line for dynamic loading with k_h =0.25 condition. This average value of k_h is obtained from the backfill accelerations of all test cases. In the static relationship, increasing the area of CDM block up to about 10 m^2 gently reduces the deflection of the quay wall, which then reduces to the lowest deflection quickly. In the dynamic relationship, on the other hand, deflection decreases rapidly up to about 40 m^2 of CDM area and then reduces to the lowest deflection. The numerical predictions agree well with the test deflections. Although the cost effective CDM size can not define in the figure, in the pseudo-static study it is observed that CDM of 2 m depth is more efficient than that of 4 m depth or full-depth in reducing the deflection of the sheet pile quay wall. In the current study the authors also observed that half-depth or the floating type CDM with larger width can be recommended for the field.

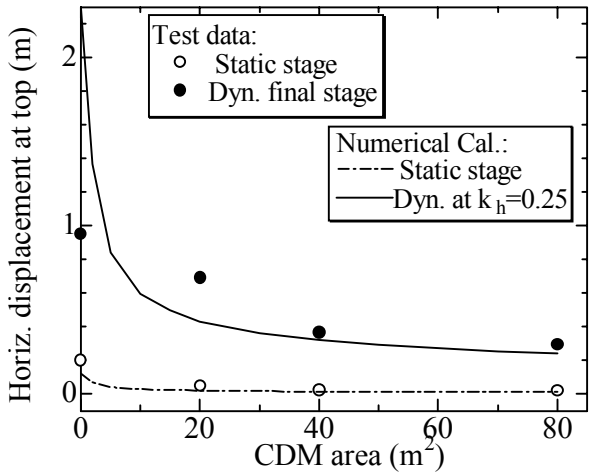

Fig. 42. Influence of area of the CDM in the horizontal displacement of the sheet pile quay wall.

Table 8. Parameters used in dynamic numerical analysis.

(a) Backfill and Bottom sand

γ_{sat} (kN/m^3)	19.6
γ_{wet} (kN/m^3)	15.9
γ' (kN/m^3)	9.8

(b) Clay Stratum

γ_{sat} (kN/m^3)	18.8
γ' (kN/m^3)	8.9
c_u (kN/m^2)	25

(c) Steel Sheet Pile Wall

I (m^4/m)	28125×10^{-8}
E (kN/m^2)	2.01×10^{8}
EI (kN.m)	56530

(d) CDM Zone

γ_{sat} (kN/m^3)	15
γ'(kN/m^3)	5.2
c_u (kN/m^2)	460

4.5 Conclusions on dynamic loaded sheet pile quay wall

A sheet pile quay wall with sea-side ground improvement has been investigated with reference to the load-deflection behavior, seismic responses, bending moment, earth pressure distribution and effect of size of cement deep mixing zone in a series of centrifuge shaking table tests. The effects of sea-side ground improvement on the stability of existing sheet pile quay wall also have been numerically predicted. Numerical predictions compare satisfactorily with the centrifuge test results. The conclusions of the dynamic loaded study are as follows:

1. Centrifuge model of a sheet pile quay wall with sea-side ground improvement is successfully established.
2. Compared with the case of a sheet pile quay wall embedded in unimproved ground, significant resistance against seismic loading is observed to develop in the CDM improved cases, i.e. the horizontal deflection is effectively reduced.

3. Acceleration motion is found consistent from the base to the top of the sheet pile quay wall system in all of the test cases and the motion is different in each shaking. In the first shaking the motion is significantly thickened from the bottom of the clay layer to the top of backfill sand or top of the clay in the sea-side. Weakening of the motion from the bottom of the clay to the top of the backfill sand or clay in the sea-side is observed in the final shaking.
4. At first shaking there is clear difference of acceleration time lag between sea-side and port-side along the depth. In higher excitation both sides also exhibit smaller to negligible time difference along the depth.
5. Excess pore pressure ratio in the clay layer is much smaller than unity, i.e., no liquefaction has taken place. Excess pore water pressure dissipates quickly, though some amount of the residual pore water pressure remains in the clay.
6. The maximum bending moment of the quay wall takes place approximately at the mid of the clay ground both in the improved and unimproved grounds. The ground improvement can reduce 30% to 60% bending moment during the seismic loading.
7. The horizontal deflection of the quay wall decreases rapidly with the increase in the area of CDM until it reaches a certain limit.
8. Proposed numerical model of the sheet pile quay wall by can predict the effect of the sea-side ground improvement in seismic loading. Prediction by the numerical model agrees fairly well with the results of centrifuge model tests.

Concluding Remarks

The stability of sheet pile quay walls on a thick clay deposit against *pseudo-static* and dynamic loading was studied through two series of centrifuge model tests. According to the tests, the improved area provided significant resistance against static and dynamic loading. The ground improvement can considerably reduce bending moment during the dynamic loading. The horizontal deflection of the quay wall decreases rapidly with the increase in area of the CDM until it reaches a certain limit.

The research indicates the possibility of modifying the current design on the DM improved ground for shett pile quay wall more reasonably and economically. Further research efforts are required to brush up and improve the current design.

Acknowledgements

The authors acknowledge the Ministry of Land, Infrastructure and Transport, Japan for providing the financial support in pursuing the study. The authors are also thankful to Mr. K. Maruyama of Geo-design Co. Ltd. who cooperated in this research significantly.

(Received on August 13, 2007)

References

Arulanandan, K. and Scott, R.F. (eds.). (1993) : *Proc. Int. Conf. on Verification of Numerical Procedures for the Analysis of Soil Liquefaction Problems*, U.C. Davis, Vol. 1. Balkema, Rotterdam.

Arulanandan, K. and Scott, R.F. (eds.). (1994) : *Proc. Int. Conf. on Verification of Numerical Procedures for the Analysis of Soil Liquefaction Problems*, U.C. Davis, Vol. 2. Balkema, Rotterdam.

Bowles, J.E. (1974) : *Analytical and Computer Methods in Foundation Engineering*, McGraw-Hill Book Co., NY.

Chang, Y.L. (1937) : Discussion of 'Lateral pile loading tests by L.B. Feagin', *Transactions of ASCE*, Vol. 102, pp. 272-278.

Coastal Development Institute of Technology (CDIT), Japan, (2002) : *The deep mixing method - principle, design & construction,* Balkema, Rotterdam.

Japanese Geotechnical Society (JGS), Japan, (2000) : *Standards of Japanese geotechnical society for laboratory shear test*, JGS, Tokyo, Japan.

King, G.J.W. (1994) : The interpretation of data from tests on laterally loaded piles, *Proc. Conf. Physical Modelling in Geotechnics*, *Centrifuge'94*, Singapore, pp. 515-520.

Kitazume, M. (1998) : Centrifuge model tests on failure of cement stabilized fly ash ground, *Soils and Foundations*, Vol. 38, No. 3, pp. 143-152.

Kitazume, M., Hayano, K., and Hashizume, H. (2003) : Seismic stability of cement treated ground by tilting and dynamic

shaking table tests, *Soils and Foundations*, Vol. 43, No. 6, pp. 125-140.

Kitazume, M., and Miyajima, S. (1995).: Development of PHRI Mark II geotechnical Centrifuge, *Technical Note of the Port and Harbour Research Institute*, No. 817, 33p.

Kitazume, M., Sato, T., Shiraishi, N. and Okubo, Y. (2002) : Failure pattern and earth pressure of locally cement improved ground under earthquake motion, *Proc. Conf. Physical Modelling in Geotechnics*, Phillips, Guo & Popescu (eds.), St. John's, Canada, pp. 581-586.

Mayne, P.W. and Kulhawy, F.H. (1982): K_0 – OCR relationships in soil, *Journal of Geotechnical Engineering Div*., ASCE, Vol. 108, No. G76, pp. 851-872.

Nippon Steel Corporation, Japan (1998): *Steel Sheet Pile – Design and Manufacture (Kou Ya ita) Nippon Steel Corporation Hand book*, p.465, (In Japanese).

Ohmaki, S., Saeki, K., Kuroda, K. and Kenmochi, S. (2002) : Sheet pile mooring wharfs in soft ground: centrifugal loading tests, *Proc. International Conference on Physical Modelling in Geotechnics*, Phillips, Guo & Popescu (eds.), St. John's, Canada, pp. 859-864.

Okabe, S. (1924) : General theory on earth pressure and seismic stability of retaining wall and dam, *Journal of Japan Society of Civil Engineers*, Vol. 10, No. 6, pp. 1277-1323.

PIANC, International Navigation Association (2001): *Seismic Design Guidelines for Port Structures*, Balkema, Rotterdam.

Rowe. P.W. (1952): Anchored sheet pile walls, *Proc. Institution of Civil Engineers*, Vol. 1, No. 1, pp. 27-70.

Takahashi, H., Kitazume, M., Ishibashi, S. and Yamawaki, S. (2006) : Evaluating the saturation of model ground by P-wave velocity and modelling of models for a liquefaction study, *International Journal of Physical Modelling in Geotechnics*, Vol. 6, No. 1, pp. 13-25.

Tschebotarioff, G.P. (1949): Large scale earth pressure tests with model flexible bulkheads, *Final Report to Bureau of Yards and Docks U.S. Navy*, Princeton University.

Tsuchida, H. (1990): Japanese experience with seismic design and response of port and harbor structures, *Proc. POLA Seismic Workshop on Seismic Engineering,* Port of Los Angeles, pp.138-164.

Tsuchida, T., Kikuchi, Y., Yamamura, K., Funada, K. and Wako, T. (2001) : Slice method for earth pressure analysis and its application to light-weight fill, *Soils and Foundations* (domestic edition), Vol. 41, No. 3, pp. 95-105 (in Japanese).

Tsuchida, T., Okumura, T., Takeuchi, D. and Kishida, T. (1996) : Development of light-weight fill from dredging, *Proc. 2nd International Congress on Environmental Geotechnics*, pp. 415-420.

Watabe, Y., Imamura, S., Hirano, T., Kishi, M. and Yamamura, K.(2006) : Seismic performance of anchored sheet pile quay wall, *Proc. 6th International Conference on Physical Modelling in Geotechnics*, Ng, Zhang & Wang(eds.), Hong Kong, 2, pp. 1119-1124.

Watabe, Y., Itou, Y., Kang, M.-S. and Tsuchida, T. (2004) : One-dimensional compression of air-foam treated light-weight geo-material in microscopic point of view, *Soils and Foundations*, Vol. 44, No. 6, pp. 53-67.

Watabe, Y., Tsuchida, T., Imamura, S. and Satoh, T. (2002) : Stability of quay wall backfilled by lightweight geo-material during earthquake, *Proc. Conf. Physical Modelling in Geotechnics*, Phillips, Guo & Popescu (eds.), St. John's, Canada, pp. 435-440.

Whitman, R.V. and Christian, J.T. (1990): Seismic response of retaining structures, *Proc. POLA Seismic Workshop on Seismic Engineering,* Port of Los Angeles, pp.427-452.

Wroth, C.P. (1984): The interpretation of in situ soil tests, 24th Rankine lecture, *Geotechnique*, Vol. 34, No. 4, pp. 449-489.

港湾空港技術研究所報告　第46巻第4号

２００７．12

編集兼発行人　独立行政法人港湾空港技術研究所

発　行　所　独立行政法人港湾空港技術研究所
横須賀市長瀬３丁目１番１号
TEL. 046(844)5040　URL. http://www.pari.go.jp/

印　刷　所　株式会社 ポートサイド印刷

Copyright Ⓒ（2007）by PARI
All rights reserved. No part of this book must be reproduced by any means without the written permission of the President of PARI.
この資料は、港湾空港技術研究所理事長の承認を得て刊行したものである。したがって、本報告書の全部または一部の転載、複写は港湾空港技術研究所理事長の文書による承認を得ずしてこれを行ってはならない。